

OPEN

A Deep Learning Framework for Design and Analysis of Surgical Bioprosthetic Heart Valves

Aditya Balu, Sahiti Nallagonda, Fei Xu , Adarsh Krishnamurthy *, Ming-Chen Hsu & Soumik Sarkar

Bioprosthetic heart valves (BHVs) are commonly used as heart valve replacements but they are prone to fatigue failure; estimating their remaining life directly from medical images is difficult. Analyzing the valve performance can provide better guidance for personalized valve design. However, such analyses are often computationally intensive. In this work, we introduce the concept of deep learning (DL) based finite element analysis (DLFEA) to learn the deformation biomechanics of bioprosthetic aortic valves directly from simulations. The proposed DL framework can eliminate the time-consuming biomechanics simulations, while predicting valve deformations with the same fidelity. We present statistical results that demonstrate the high performance of the DLFEA framework and the applicability of the framework to predict bioprosthetic aortic valve deformations. With further development, such a tool can provide fast decision support for designing surgical bioprosthetic aortic valves. Ultimately, this framework could be extended to other BHVs and improve patient care.

Semilunar valves (i.e. the aortic and pulmonary valves) are structures that permit blood to be pumped into the aorta and pulmonary artery from the ventricles during systole, and prevent backflow into the ventricles during diastole¹. Valvular heart disease is clinically characterized either by gradual narrowing of the valve due to calcification of the leaflets or regurgitation through the valve due to insufficient valve closure². Valve repair and replacement are two possible interventions to address diseased valves and prevent congestive heart failure or death. Based on the estimates from the American Heart Association, more than 2.5% of the United States population is affected by valvular heart diseases³. Heart valve replacement is common for patients suffering from valvular heart valve disease; over 90,000 prosthetic heart valves are implanted in the United States every year⁴. One of the most popular classes of replacement valves are surgical bioprosthetic heart valves (BHVs), fabricated from chemically-treated biological tissues². They provide better hemodynamic characteristics than mechanical prostheses (the other most popular class), but are prone to fatigue failure, limiting their durability to 10–15 years. However, estimating the remaining life of a BHV directly from medical images is difficult. On the other hand, valve performance measures can be used by physicians to make better valve replacement decisions, preventing premature replacements or surgeries^{5,6}.

Computational analysis of the heart valve can be an important tool in understanding the etiology of valvular diseases and can help clinicians in obtaining additional information that aid in therapeutic or valve replacement decisions. For example, the failure of aortic valves can be related to stress concentration in the leaflets of the BHV⁷. Heart valve analysis using computational models has been extensively studied in recent years^{2,7–11}. A review of computational modeling methods that have been developed to provide diagnosis from medical images for aortic valves is presented by Zakerzadeh *et al.*⁹. Several quantities of interest can be obtained and studied from these computational models. Two key quantities of interest are the coaptation area, which reflects of the degree of valve closure, and the effective orifice area (or open area), which reflects the degree of valve opening. The closure of the heart valve can be assessed by performing structural analysis of the valve geometry with appropriate boundary conditions to simulate the valve closure. Similarly, the effective orifice area can be computed by performing valve opening simulation or dynamic simulation of the valve for one complete cycle of the heart beat^{9,10}. In this paper, we restrict our focus to valve closure simulations; however, our framework can be extended to dynamic simulations for obtaining other quantities of interest such as effective orifice area.

An accurate representation of the heart valve geometry is essential to assess its performance. Non-uniform rational B-splines (NURBS)¹² have been the de facto standard for geometry representation in mechanical

Iowa State University, Department of Mechanical Engineering, Ames, Iowa, 50011, USA. *email: adarsh@iastate.edu

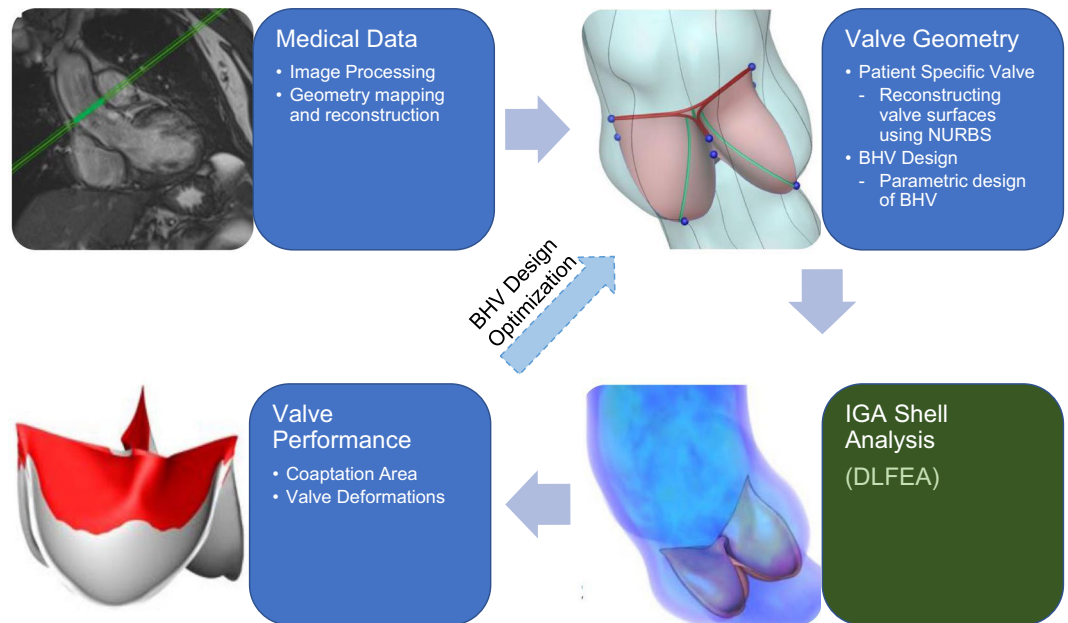


Figure 1. A framework for predictive biomechanics-based approach for design of BHVs. Evaluating the valve performance using finite element analysis is a critical time-consuming step in the process. DLFEA can replace compute intensive biomechanics simulations with fast valve performance evaluations.

computer-aided design (CAD). NURBS surfaces can be used to parametrically design complex geometric objects, while allowing easy modifications. Current state-of-the-art valve analysis approaches reconstruct the aortic heart valve geometry from computed tomography (CT) images using NURBS^{5,10}. In addition, current BHVs are designed only for certain discrete population-averaged sizes. These geometries are then analyzed using shell formulations of finite element analysis after meshing to assess the valve performance⁵. One of the most promising new analysis technologies that can be also used for valve simulations is isogeometric analysis (IGA)¹³. IGA unites engineering analysis and design by eliminating the tedious process of finite element mesh generation from the design geometry. IGA uses the B-spline basis functions for both representing the geometry and for the analysis. Hence, the NURBS valve geometry can be directly used for both valve design and analysis using IGA^{10,14–17}.

The complete pipeline for the design and analysis of heart valves is illustrated in Fig. 1. While these analysis frameworks have proven to be useful, they often involve large computational overhead. Deep learning can provide a viable fast alternative to computational analysis, specifically IGA, to accelerate the design and analysis process for bioprosthetic valves. Deep learning has emerged as a major machine learning paradigm that has demonstrated transformative potential in many areas of science and engineering¹⁸. In sciences, the applications range from astronomy¹⁹, high-energy physics²⁰ and material science^{21–23} to medical diagnostics²⁴ and plant sciences²⁵. In the domain of engineering, deep learning is the key enabler of the recent autonomous driving revolution²⁶ along with other significant progresses in robotics²⁷, design and manufacturing^{28,29} and prognostics and health management of engineered systems³⁰. Along with recent algorithmic advances, the success of deep learning as a powerful function approximator could be attributed to the availability of large volume of data and advances in high-performance computing such as the Graphics Processing Units (GPUs).

In this work, we leverage the advances in deep learning to overcome the computational overhead in analysis of heart valves and to make valve design decisions. Note that in this work, we only specifically refer to surgical aortic valves with a stent that is sutured to the aortic root. Specifically, we propose a deep-learning-based convolutional autoencoder architecture (referred to as DLFEA) for predicting the analysis output directly from the input heart valve geometry. This approach accelerates the analysis by acting as a surrogate model that can be trained using previous analyses of multiple simulations. In particular, as a proof of concept, we predict the final deformed closed shape of the heart valve and the coaptation area, a key quantity of interest for surgeons. Coaptation area has been widely used as a key valve performance metric in the design and diagnosis of heart valves and predicting it has been the focus of several previous studies⁵. The stresses and strains during the heart valve closure can be directly computed from the heart valve deformations. However, the proposed methodology is general; it can be extended to analyze other key performance characteristics of heart valves and more complex valve simulations that include fluid structure interaction^{10,15–17,31}.

We have the following specific contributions: (i) a deep learning framework, DLFEA, to predict the deformation biomechanics of aortic valves trained using isogeometric analysis simulation data; (ii) a novel geometric analysis tool called *NURBS-aware convolution* to directly input the valve geometry information to the deep-learning model; and (iii) statistical and anecdotal results that establish the accuracy and robustness of the proposed method. Please refer to the *Related Works* section in the Methods for a detailed discussion of our contributions in the context of recent advances in machine-learning based surrogate modeling for simulations. The results suggest that the DLFEA framework can be directly used in the design and optimization of patient-specific BHVs.

Stats	Euclidean			Hausdorff			Procrustes		
	Max.	Mean	Median	Max.	Mean	Median	Max.	Mean	Median
Training	0.1546	0.0173	0.0122	0.2908	0.0830	0.0779	0.0206	0.0021	0.0015
Validation	0.1337	0.0173	0.0120	0.2444	0.0827	0.0778	0.0173	0.0021	0.0014
Test	0.1502	0.0173	0.0119	0.2897	0.0821	0.0770	0.0204	0.0021	0.0014

Table 1. Statistics on the metrics of deformations predicted by the DLFEA. All metrics are in cm.

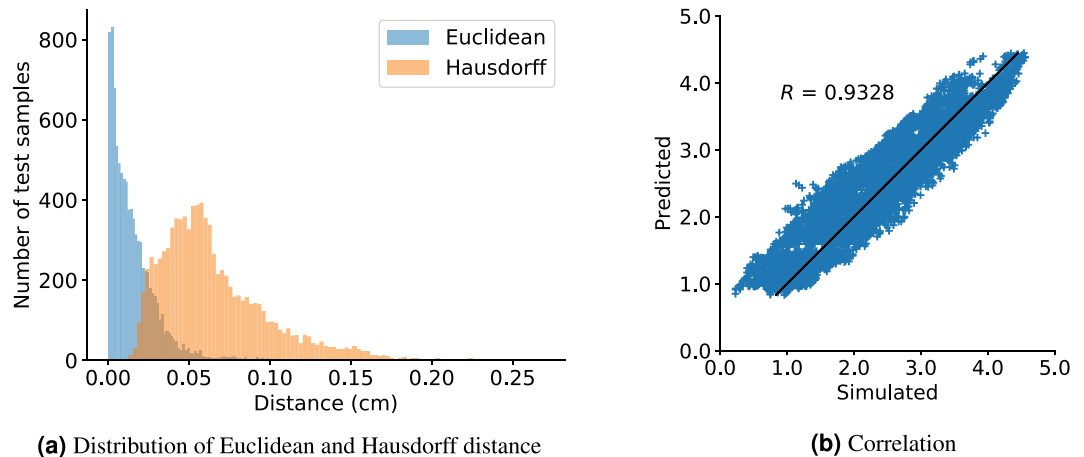


Figure 2. The histograms (a) show the Euclidean distance and Hausdorff distance between predicted deformations from DLFEA and the simulated deformations for the test data. (b) Shows the DLFEA-predicted coaptation area compared with the coaptation area obtained from simulations. The predicted coaptation area is highly correlated ($R = 0.9328$) with the simulated values.

Results

The DLFEA framework predicts the final deformations of the aortic valve and the valve coaptation area using the original undeformed geometry of the valve, the aortic pressure, and the material properties of the valve as input. We performed 90,941 valve closure simulations by varying the undeformed geometry, pressure, and material properties. Of these simulations, 72,753 simulations were used for training the DLFEA; 9,094 simulations for validating the training and hyperparameter tuning; and the rest for testing. We compare the performance of DLFEA framework on a test dataset (containing results from 9,094 simulations), which were not used for training.

The DLFEA framework can accurately predict the valve deformations. The valve deformations were compared using three metrics: Euclidean distance, Hausdorff distance, and Procrustes matching (see Table 1). The average Euclidean distance between the predicted and simulated valve deformations is 0.0649 cm (note the average diameter of a heart valve is 2.3 cm³²). An histogram of the Euclidean and Hausdorff distances between the predicted and simulated deformed valve geometry is shown in Fig. 2(a). In addition, the DLFEA can also accurately predict the valve performance quantities of interest; in this case the coaptation area. The root mean squared error and the correlation between the predicted and the simulated coaptation area is 0.1167 cm² and 0.9328, respectively (see Fig. 2b).

We present some anecdotal BHVs to understand the generalization capability of the trained model. We visualize the predicted and simulated deformed geometry of the leaflets and the strains computed using the simulated and predicted deformations in Fig. 3.

Finally, we also visualize the high-dimensional data manifold using t-distributed stochastic neighbor embedding (t-SNE)³³. We perform this by analyzing the correlation between the learned information vector from DLFEA (the output of fusion layer in DLFEA, also called the code layer of an autoencoder) and the features of the input. In Fig. 4, we show the 2D embedding colored based on different geometric parameters (belly curve parameter, free edge curve parameter, and height of free edge, which were used to obtain different reference configurations) to understand the correlation between the data manifold and the valve geometry.

Discussion

The results presented in the above section show that the DLFEA framework is able to accurately capture the deformation biomechanics to within reasonable error bounds. The maximum value of the displacement among all the valve leaflets from the simulations is 0.7642 cm. The maximum Hausdorff distance (which is the maximum among all measures) between the predicted and simulated valve displacements is within 15% of this maximum displacement. In addition, the median and mean value is less than 5% of the maximum displacement.

The predicted and simulated deformations are visually quite similar with some minor regional differences that are within $\approx 10\%$ error, which is usually within the measurement accuracy of non-invasive imaging modalities such as Echocardiography³⁴. In addition, the deformations predicted by DLFEA are accurate and smooth enough

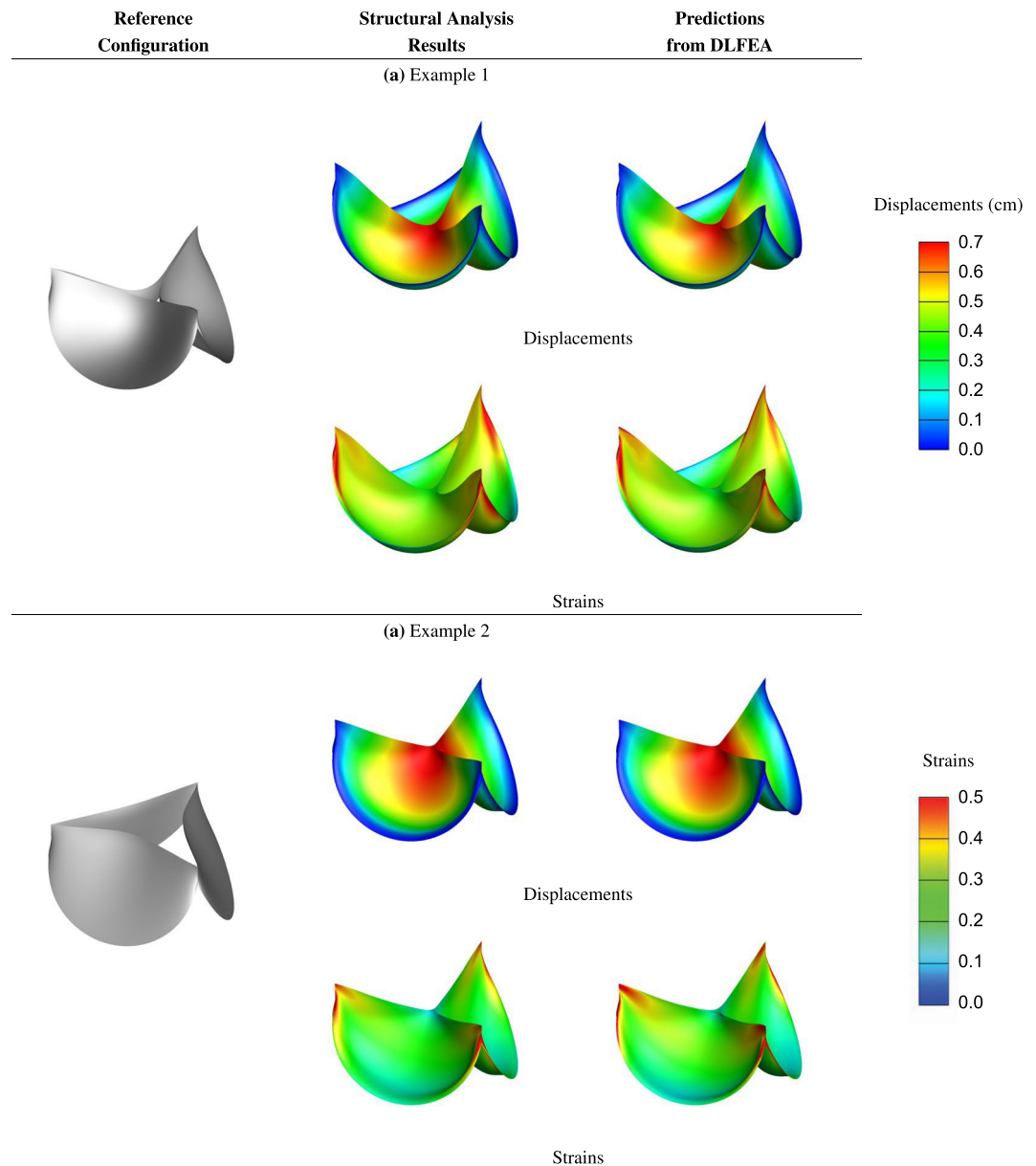


Figure 3. Illustrative examples of valve deformations and their corresponding maximum in-plane principal Green-Lagrange strains computed from isogeometric simulations and the predicted deformations using the DLFEA framework.

that the strains calculated from them are also smooth without any oscillations. More interestingly, we find that the DLFEA is able to learn certain complex interaction characteristics of the leaflets and their deformations. The predictions by DLFEA capture the symmetry of the three leaflets without any explicit training constraints. The DLFEA also captures the contact characteristics between the three leaflets accurately without any explicit information about contact mechanics (for example, penalty for interpenetrating leaflets).

The t-SNE embedding is the lower dimensional representation of the data manifold and if the network is properly trained, this embedding is the representation of the original data-manifold in a compact lower dimensional space that nearly preserves the distance metric³⁵ (that is, similar input data are close in the t-SNE embedding). In the t-SNE embedding of our DLFEA network (Fig. 4), we see that this compact lower-dimensional space represents the complete variation in the data (design) space (i.e. the behavior of the valve deformation due to all the input parameters is well learnt). The local clustering of the training data in the t-SNE visualizations based on the geometric parameters demonstrate that the machine learning network has learnt the underlying geometric parameters of the valve. For example, in Fig. 4(a), similar belly curve parameter values are clustered together. Note that the geometric parameters are not provided as input to the t-SNE algorithm; it is only used for labeling the visualization of the points. In addition, none of the geometric parameters are directly given as input to DLFEA.

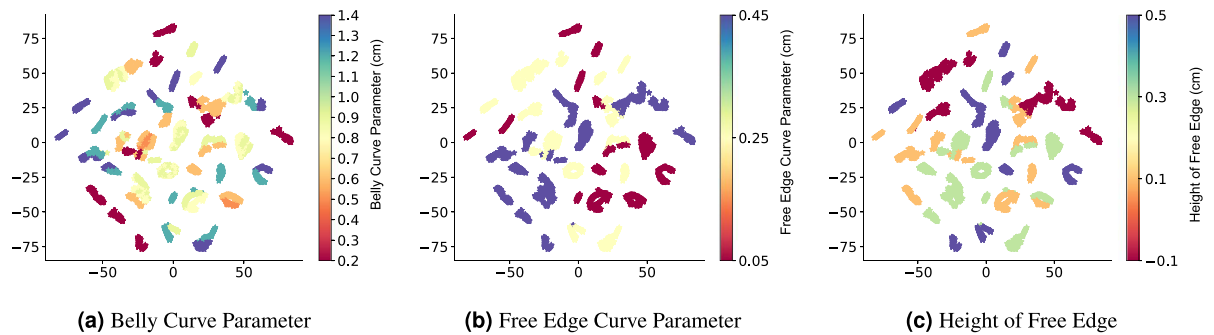


Figure 4. t-distributed stochastic neighborhood embedding (t-SNE) of the higher dimensional manifold learnt by DLFEA. t-SNE generates a lower dimensional embedding of the data using the learnt model, which can provide insights into the distribution of the data. This particular t-SNE shows that the different geometries are well clustered, showing that the model has reasonably learnt the effect of geometric parameters used for generating the reference configurations, although this information is not available to the model.

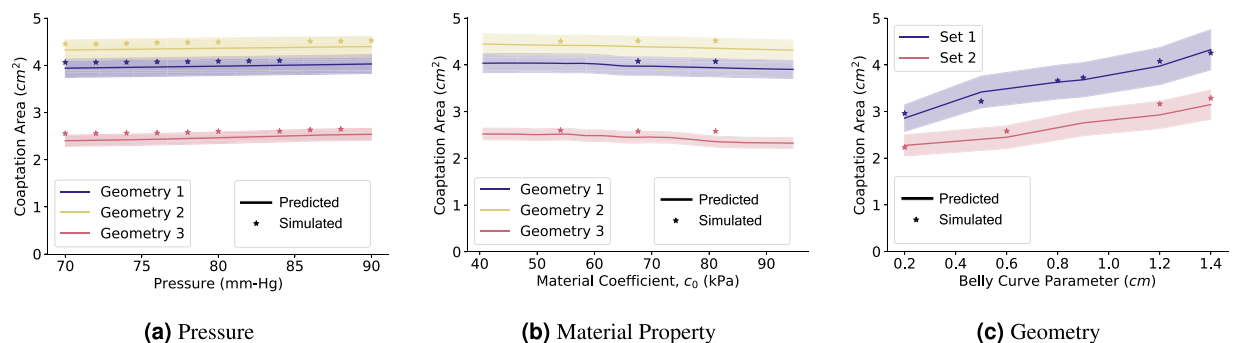


Figure 5. The DLFEA-predicted coaptation area variation with pressure is shown in (a) for three specific sets of reference configuration geometries. (b) Shows a similar plot with variation in material coefficient 1 (see Supplement for more details) for three specific reference configurations, pressure, and other material properties. (c) is a similar plot with variation in geometry parameter (belly curve parameter, see Supplement) for two specific material properties, and pressure. These plots are generated with 1000 intermediate values in the parameter of interest. The region estimating 10% variation of the predicted coaptation area value is highlighted.

The network is able to learn this relationship from the training data alone. Please refer to the Supplement for a more detailed study of the t-SNE based on the domain knowledge.

The predicted coaptation area correlates highly with the simulated value (Fig. 2(b), $R = 0.9328$). In order to further understand the efficacy of DLFEA in interpolating and extrapolating the coaptation area predictions for different parameter values, we performed an ablation study (Fig. 5). We first fixed the reference geometry and material properties to vary the pressure (Fig. 5(a)) and calculated the predicted and simulated coaptation areas. Similarly, we fixed all the parameters including geometry and varied only one of the material properties (Fig. 5(b)). Finally, we performed a similar study for one of the geometric parameters (Fig. 5(c)). The predicted values are generated by densely varying the corresponding parameter in the physiological range (with 1000 intermediate values, for example, pressure is varied uniformly from 70 mmHg to 90 mmHg with an increment of 0.2 mmHg to generate 1000 data points). We also chose a few random parameter values and performed the valve closure simulations to compute the simulated coaptation area. This experiment was repeated for several parameter sets. In Fig. 5, we also highlight the region estimating 10% variation of the coaptation area value from the predicted values. The difference between the simulated and predicted values are within this 10% error margin. Moreover, the predicted values smoothly capture the overall trend of the change in the coaptation area with respect to the different parameters, without any artifacts. This demonstrates the generalization capability of the network for any parameter value in the physiological range. Such a generalization capability over parameters such as belly curve parameter is an interesting outcome from the hierarchical learning of deep learning from the raw geometric representation. Finally, this shows that such a system can be used as a fast function evaluator for an optimization system, which can be used to design optimal prosthetic valve geometries.

There are some limitations to the current implementation of the study. We do not account for anisotropy of the valve tissue material, which needs to be considered for more accurate modeling of the valve deformations. In order to make the study patient-specific, a large amount of patient data covering the geometry variation of aortic valve among a diverse set of population is needed. In addition, the BHV design parameter space needs to be validated to make sure that the resulting valve designs cover the complete geometry variation in the valves

of these patients. Finally, new methodology that is accurate in handling cases with out-of-distribution samples while performing inference needs to be developed. These improvements would make the system practical for patient-specific valve design.

In conclusion, we have presented a deep-learning-based framework to predict the deformation biomechanics of heart valve that are not directly captured using medical imaging and often require elaborate computational expertise and cost to determine. We have demonstrated the capability of this methodology to learn complex deformation biomechanics of the heart valves with different geometry, material properties, and boundary conditions. This makes the framework directly useful for parametric design of BHVs. Such a fast decision support system can enable development of personalized heart valve designs with better fit and performance, ultimately improving patient care.

Methods

Deep Learning, a subset of machine learning approaches, has emerged as a versatile function approximator that can establish a reliable map between (possibly heterogeneous) inputs and outputs of complex phenomena. A deep neural network is made up of several layers l_i , which takes as input x_{l_i} and produces an output $y_{l_i} = \sigma(W_{l_i} \cdot x_{l_i} + b_{l_i})$, where $\sigma(\cdot)$ represents a non-linear activation function, W_{l_i} and b_{l_i} are the weights and biases, respectively, for connecting the input neurons to the output neurons. The connections could be as simple as a dense connection between every input neuron and output neuron. However, dense connections may fail to preserve local correlations in input that may encode useful information, for example, in the case of image classification. Furthermore, learning the dense connectivity between the neurons increases the sample complexity and all connections may not be meaningful. A convolutional connection instead of a dense connection helps alleviate these issues. The convolution operation (\otimes) is given by

$$W[m, n] \otimes x[m, n] = \sum_{i=-h}^{i=h} \sum_{j=-l}^{j=l} W[i, j] x[m - i, n - j]. \quad (1)$$

Recently, deep learning has been successfully deployed in several areas with newer and more sophisticated architectures such as variational autoencoders^{36,37}, generative adversarial networks³⁸, graph convolutions³⁹, etc. Once the network architecture is defined, the network weights (that are initialized randomly) are updated using the back-propagation algorithm⁴⁰ based on minimizing a loss metric. At the end of training, the best weights and biases that generate the minimal prediction loss are chosen for the network. This network can then be used to predict the outputs for the test inputs.

Related Works. Deep learning applications to create surrogate models for finite element analysis is a very recent area of research that specifically focuses on bridging physics based models and data-driven models. Some of the recent advances in this research area are summarized below:

1. **Physics-consistency in deep learning:** The overall idea is to merge the ideas of deep learning and physics by using physics-based features while training the deep learning models. For example, researchers have modified the loss functions to ensure some physical constraints are satisfied^{41–45}. There has also been work on interpreting the predictions of the deep learning model based on physical conditions^{22,23}.
2. **Incorporating partial differential equations (PDEs) in deep learning models:** The key idea is to use the underlying governing equations such as Berger's equation, Navier-Stokes equation, Cahn-Hilliard's equation, etc. to compute the residual for the sample. Since modern software systems can define these partial differential equations numerically in terms of automatic differentiable functions, it is easy to minimize these residuals. There are several recent works on learning from partial differential equations^{22,46–51}.
3. **Generative vs. distinctive predictions:** While there are methods in Deep Learning for generating and even predicting desired outputs, the underlying physics is often more strict. For example, given a set of physical conditions (such as loads on a well-defined geometry) will result in a deterministic desired output (such as displacements). Modeling them as a generative model is not consistent with the physics. On the contrary, the inverse problem, of defining the displacement of a given geometry and predicting the set of physics conditions is often ill-posed and could be consistently modeled as a generative model. There are several works showing the capability of Deep Learning methods to act as a surrogate^{23,41,49,51}. These surrogates are modeled as distinctive (non-generative) networks, since the physics is deterministic and the problem is well-posed. On the contrary, there are some recent works^{22,42,46}, which deal with stochastic PDEs or with ill-posed problems such as inverse design which demand the use of a generative model.

In the application area of biomechanics, most of the existing works use simple deep learning or physics-consistent deep learning methods. Specifically, these methods have been applied for modeling the aorta and estimating the stress fields^{52–54} or estimating the constitutive model parameters for aortic wall^{55,56}. For BHVs, while there are optimization based methods for design of transcatheter aortic valves^{57,58}, machine learning methods have mainly been used for 3D reconstruction of the valve geometry⁵⁹. Further, there are physics-informed deep learning approaches for modeling cardiovascular flows, which incorporate residual minimization of the PDEs using deep learning^{60,61}. However, to the best knowledge of the authors, deep learning has not been used for analyzing the deformation behavior of bioprosthetic valves.

In this work, we leverage the advances in deep learning to model the analysis of BHVs and to accelerate their design. The efforts made in physics-consistent deep learning and deep learning applications to biomechanics

motivates this work. While there are several works in this fast growing area, there are still some gaps which are yet to be filled. This paper addresses some of those gaps:

1. **Predicting raw values vs. descriptors for biomechanics applications:** The current state-of-the-art machine learning works in biomechanics directly predict the stress field. However, during the physics solve, the stresses are not directly obtained. While it is challenging to obtain displacements from stresses, it is straight-forward to obtain the stresses and strains from displacements. Even though, small variations in the displacements can lead to large oscillations in the strain computations, in our case (see Fig. 3), the maximum principal strain obtained from predicted deformations is accurate and without any numerical oscillations. Therefore, we attempt to be consistent with the way physics is modeled to enable future work in using PDEs for computing residuals. Incorporating PDEs for modeling the complex dynamics involved in the bioprosthetic aortic valves is not a trivial extension of the present work, but, this contribution is a step forward towards that end.
2. **Contact prediction in deep learning:** Current physics consistent deep learning models and deep learning for biomechanics applications consider simple cases which doesn't involve interaction of multiple objects (or multiple features of the same object). This is important when we need to model contact physics among the objects. This is necessary in BHVs while predicting the contact between the leaflets. As seen in the Figures shown in Fig. 3, our method is able to learn the complex interaction of the three leaflets which is necessary while modeling the non-smooth behavior of the materials.
3. **Accurate representation of 3D geometries:** In general, there is a disconnect between the geometry, the physics domain mesh, and the data representation for training physics consistent deep learning model. Converting one form of data to another is computationally expensive and not accurate. To avoid this, often researchers use a structured mesh which could be expensive in case of representing geometries with complex geometric features such as the heart valve. On the contrary, we make use of a NURBS-aware convolution operation and isogeometric analysis to alleviate this issue.

Deep-Learning for finite element analysis (DLFEA). Learning the deformation biomechanics of heart valves involves learning multiple physical phenomena by the DLFEA framework. First, the DLFEA needs to learn from the input 3-dimensional Euclidean space geometry and predict the deformed shape also in 3-dimensional Euclidean space. Next, it needs to learn the effect of loads and boundary conditions on the deformation. It should learn about the interaction between the leaflets during closure (often dealt with by using a complex contact algorithm in traditional finite element analysis) to predict the coaptation area. Finally, it should learn the material behavior and the dependence of the deformation on the thickness of the leaflets used in the simulation.

Any machine learning framework requires the identification of three main components: (i) data representation, (ii) model architecture, and (iii) training algorithm. In the following subsections, we describe the different components of our DLFEA framework. Please refer to the supplement for details regarding parametric design of heart valves and simulation of valve closure using IGA. These methods were used for training data generation for the DLFEA framework.

Data representation. Learning directly from 3-dimensional Euclidean space is an interesting notion that has been explored extensively in machine learning literature. There are traditional approaches of object recognition using a 3D volume occupancy grid⁶² or its extensions such as Octrees⁶³ and multi-resolution voxels⁶⁴. Further, another class of algorithms have been developed to learn from point clouds⁶⁵. There are other approaches where the topology of the data is modeled as a graph to perform a graph convolution operation³⁹. However, the above mentioned methods have high sample complexity or time complexity for learning. Moreover, there is loss of information while transforming the CAD model to other representations. Hence, integrating the learning paradigm with the CAD representation is crucial. To this end, we propose a new NURBS-aware convolution operation.

The crux of the NURBS-aware convolution operation is to perform the convolution operations on the NURBS control mesh of the input geometry to obtain the valve performance measures. The control points of NURBS surfaces provide the 3D surface representation of BHVs. Hence, for extracting the geometry information from different heart valves, it is sufficient to utilize the control points directly for the convolution operation. The control points can be represented as a rectangular matrix representing the tensor-product structure of these valve surfaces. Since, these control points are physically significant and are represented in the 3D Euclidean space, they can be represented as three different matrices with each of them containing the position with respect to each coordinate as shown in Fig. 6. This is equivalent to representing the control points as a RGB texture⁶⁶. This method was used earlier to perform fast and parallel GPU evaluation of NURBS surfaces. Here, using this representation of the leaflet, we perform the convolution operation directly using the NURBS surface without any loss of information, and can learn using traditional convolutional neural networks. A similar mapping is required for deconvolving the final deformed geometry from the textural representation to the global coordinates.

Model architecture. We use convolutional autoencoder-type architecture to obtain the deformed geometry for a given heart valve. The autoencoder architecture is composed of three main components: (i) an encoder network, (ii) a code layer and (iii) a decoder network (see Fig. 7). An encoder network is designed to compress high dimensional input data into a lower dimensional embedding. The dimension of the embedding is very important since while a smaller dimensional embedding represents a succinct noise-less representation of the inputs, it also leads to a greater loss of information. This low dimensional embedding is represented in the code layer. Using this, one could generate/reconstruct the original high dimensional representation using a decoder network. An end-to-end

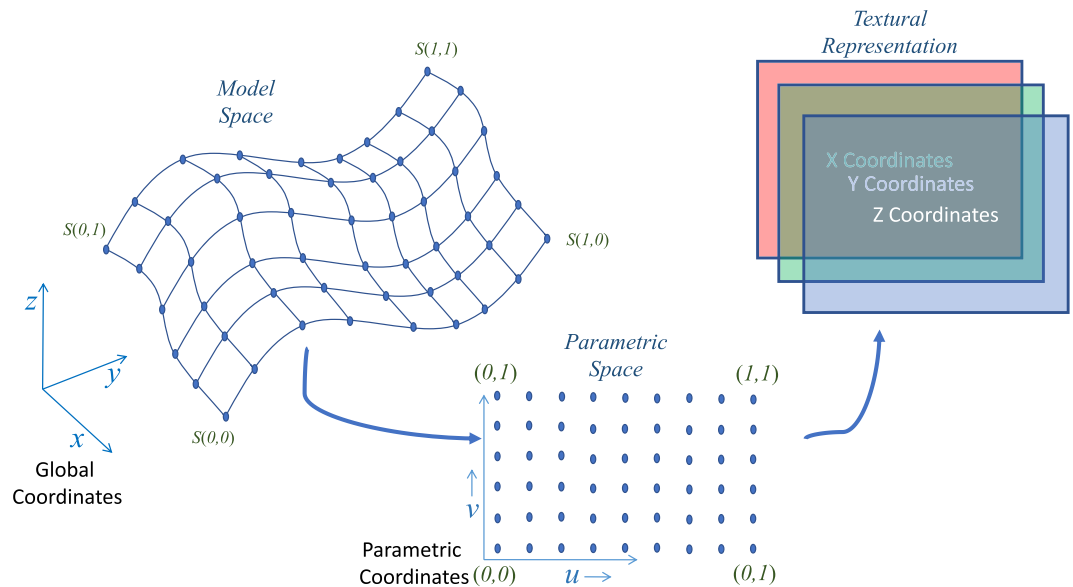


Figure 6. NURBS-aware convolution. In order to learn from a 3D surface, we extract the control points of the NURBS surface in the parametric space, which introduces spatial structure to the control points. We restructure the control points (from the parametric space) into three channels of an image (texture representation) to perform traditional convolution operations.

training using the reconstruction loss is used to train the entire autoencoder. This method has been shown to quite effective for denoising and enhancing images and videos for computer vision^{37,67}.

We split the heart valve into three leaflets and for each leaflet, we use the NURBS-aware convolution operation where the NURBS surface is represented using three rectangular matrices (of size $m \times n \times 3$, where m and n are the number of control points in both directions of the parametrization). Now, using this data representation, we convolve further using traditional convolutional layers to create the encoder block of the autoencoder^{36,37}.

Thus, using an encoder, we represent the high dimensional surfaces to an informative lower dimensional representation. We then fuse the information of features obtained from the encoder for the three leaflets by flattening the low-dimensional output and connecting all the outputs using a fully connected layer. This is required to learn the interaction between the three leaflets, such as contact or closure of the leaflets. However, this increases the sample and time complexity of training due to the increase in the number of weight parameters. However, since we perform this operation in the low dimensional manifold, the increase in complexity can be accommodated efficiently. Ensuring the correct size of the code layer of the encoder is necessary, since there is a trade-off between complexity and performance. We vary the size of the code layer until we get the best performance for a set of samples.

Apart from the interaction, the deformation biomechanics depends on the material properties of the heart valve which are also used in the simulations. Uniform pressure is applied on the heart valve as a boundary condition. At the closed state, the valve is in a hydrostatic state of stress, where the loading is uniform in all directions. Hence, a scalar pressure value is sufficient to correctly define this boundary condition. However, in order to ensure that the scalar plays significant role in learning, we repeat the scalar pressure value multiple times to form a vector of size 10 (obtained after experimentation). We fuse the material properties vector and pressure boundary condition of the heart valve (pressure vector) with the fused embedding (fully connected layer obtained earlier) of the leaflet geometry.

Since the coaptation area is an important functional parameter used to determine the BHV health, we chose to predict this quantity of interest directly using the network. We also chose to predict the final deformed shape of the leaflet geometry, which can be used to obtain any other measures such as leaflet strains and also provide visual feedback of the deformed shape. The deformed geometry is predicted by using a decoder block which decodes the information from the fully connected layers used for fusing the information from thickness, pressure, and leaflet geometry. The decoder predicts the final deformed control points of the heart valve, which can be multiplied directly with the weights and knot vectors of the original geometry to get the deformed surfaces.

The final requirement for effective learning is to introduce a linear/non-linear activation for each output. In the case of the coaptation area, a rectified linear unit (ReLU) is the best fit, since the coaptation area is always non-negative. The ReLU function is represented as follows:

$$\text{ReLU}(x) = \max(x, 0). \quad (2)$$

On the contrary, deformations of the leaflets could be negative at some locations, which makes ReLU a bad fit to use as an activation function for this output. Hence, linear activation function is used for the deformations. In the next subsection we outline the details of training the proposed network architecture.

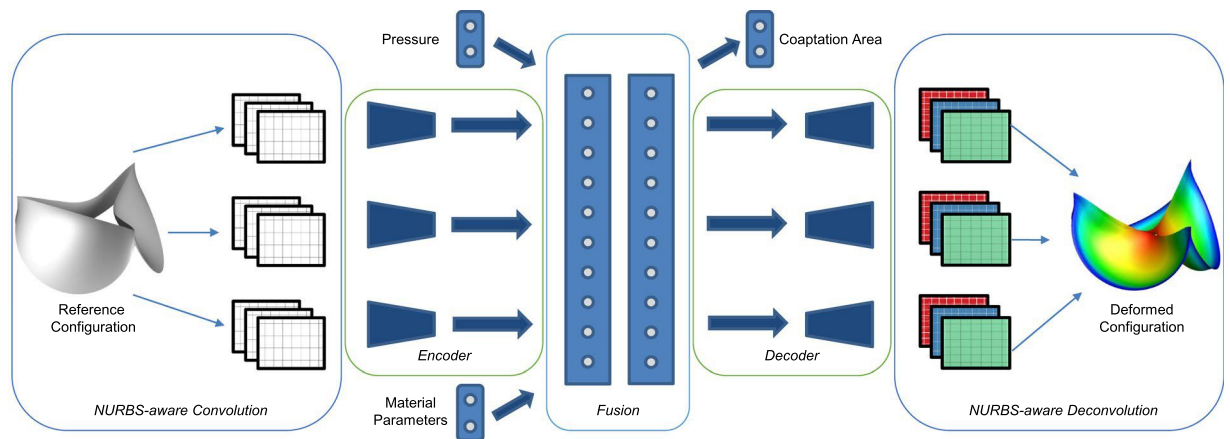


Figure 7. Deep-learning-based convolutional autoencoder for predicting the output deformations and the coaptation area of the heart valve in the closed state, with the BHV leaflet reference geometry, material properties, and the aortic pressure as input. The leaflet deformations are individually learnt using a NURBS-aware convolution followed by an encoder. All the inputs are fused using the intermediate fusion layers (also called as the coding layers).

Training algorithm. In the previous two subsections, we explained the embedding of the different physical attributes in the data representation and the machine learning model to enable effective learning. This is required for effective learning since the sample complexity and time complexity are still a challenge. Although compute capability is abundant especially with the advent of GPUs, there are still limitations on the amount of data that can be generated in a viable time frame, specifically when the data is generated from computationally heavy simulations. Hence, embedding the physical attributes in different possible ways is required for effective machine learning methods. In addition, this helps us leverage some of our physical understanding of the process, thereby reducing the learning complexity for the machine learning network.

Another important physical characteristics that we need to embed are the essential boundary conditions imposed on the geometry for valve closure. Fixed boundary conditions affect the deformation of the BHV simulations. While the fixed node has zero deformation, achieving zero predicted deformation up to an arbitrary precision is numerically difficult. Further, if the back-propagation algorithm tries to achieve that, the nodes with non-zero deformation are affected, making the overall deformation difficult to learn. We deal with fixed boundary conditions by weighing the loss with the true deformations. If the original loss function used is l , the modified loss function is

$$l_{bc} = \text{abs}\left(\frac{u_{true}}{\max(\text{abs}(u_{true}))}\right)l, \quad (3)$$

where l_{bc} represents the boundary condition incorporated loss function and u represent the displacements. In practice, we use l to be mean squared error:

$$l = \frac{1}{|\mathcal{D}|} \sum_{k \in \mathcal{D}} (u_{pred_k} - u_{true_k})^2, \quad (4)$$

where \mathcal{D} is the dataset to learn from, $|\mathcal{D}|$ is the number of data points used for training and u_{pred} and u_{true} represent the predicted and true displacements respectively.

In order to improve the sample complexity, we also perform data augmentation⁶⁸. Using arbitrary scalar values, we shift the BHV models to generate modified control points of a new BHV, which augment the original training data. We make use of a parametric BHV design algorithm (see Supplement) to generate different valve geometries. These valve geometries, along with different valve material properties and aortic pressures, are used to simulate valve closure using isogeometric analysis. Part (60%) of the simulated deformed geometries along with their calculated coaptation area are used as data for training the DLFEA framework. Of the remaining data, 20% was used for validation and 20% for testing.

Data availability

The datasets generated and/or analysed during the current study are available at <http://web.me.iastate.edu/idealab/c-dlfea.html>.

Received: 25 July 2019; Accepted: 15 November 2019;

Published online: 06 December 2019

References

- Hinton, R. B. & Yutzey, K. E. Heart valve structure and function in development and disease. *Annual review of physiology* **73**, 29–46 (2011).
- Soares, J. S. *et al.* Biomechanical behavior of bioprosthetic heart valve heterograft tissues: Characterization, simulation, and performance. *Cardiovascular Engineering and Technology* **7**, 309–351 (2016).
- Benjamin, E. J. *et al.* Heart disease and stroke statistics: a report from the AHA. *Circulation* **137**, e67–e492 (2018).
- Pibarot, P. & Dumesnil, J. G. Prosthetic heart valves: selection of the optimal prosthesis and long-term management. *Circulation* **119**, 1034–1048 (2009).
- Morganti, S. *et al.* Patient-specific isogeometric structural analysis of aortic valve closure. *Computer Methods in Applied Mechanics and Engineering* **284**, 508–520 (2015).
- Nkomo, V. T. *et al.* Burden of valvular heart diseases: A population-based study. *The Lancet* **368**, 1005–1011 (2006).
- Chandran, K. B. Role of computational simulations in heart valve dynamics and design of valvular prostheses. *Cardiovascular Engineering and Technology* **1**, 18–38 (2010).
- Croft, L. R. & Mofrad, M. R. K. Computational modeling of aortic heart valves. In *Computational Modeling in Biomechanics*, 221–252 (Springer, 2010).
- Zakerzadeh, R., Hsu, M.-C. & Sacks, M. S. Computational methods for the aortic heart valve and its replacements. *Expert Review of Medical Devices* **14**, 849–866 (2017).
- Xu, F. *et al.* A framework for designing patient-specific bioprosthetic heart valves using immersogeometric fluid–structure interaction analysis. *International Journal for Numerical Methods in Biomedical Engineering* **34**, e2938 (2018).
- Kamensky, D. *et al.* A contact formulation based on a volumetric potential: Application to isogeometric simulations of atrioventricular valves. *Computer Methods in Applied Mechanics and Engineering* **330**, 522–546 (2018).
- Piegl, L. & Tiller, W. The NURBS book (1997).
- Hughes, T. J. R., Cottrell, J. A. & Bazilevs, Y. Isogeometric analysis: CAD, finite elements, NURBS, exact geometry and mesh refinement. *Computer Methods in Applied Mechanics and Engineering* **194**, 4135–4195 (2005).
- Kiendl, J., Hsu, M.-C., Wu, M. C. & Reali, A. Isogeometric kirchhoff–love shell formulations for general hyperelastic materials. *Computer Methods in Applied Mechanics and Engineering* **291**, 280–303 (2015).
- Hsu, M.-C., Kamensky, D., Bazilevs, Y., Sacks, M. S. & Hughes, T. J. R. Fluid–structure interaction analysis of bioprosthetic heart valves: significance of arterial wall deformation. *Computational Mechanics* **54**, 1055–1071 (2014).
- Kamensky, D. *et al.* An immersogeometric variational framework for fluid–structure interaction: Application to bioprosthetic heart valves. *Computer Methods in Applied Mechanics and Engineering* **284**, 1005–1053 (2015).
- Wu, M. C. H., Muchowski, H. M., Johnson, E. L., Rajanna, M. R. & Hsu, M.-C. Immersogeometric fluid–structure interaction modeling and simulation of transcatheter aortic valve replacement. *Computer Methods in Applied Mechanics and Engineering* **357**, 112556 (2019).
- Goodfellow, I., Bengio, Y., Courville, A. & Bengio, Y. *Deep learning*, vol. 1 (MIT press Cambridge, 2016).
- Reis, I., Poznanski, D., Baron, D., Zasowski, G. & Shahaf, S. Detecting outliers and learning complex structures with large spectroscopic surveys—A case study with APOGEE stars. *Monthly Notices of the Royal Astronomical Society* **476**, 2117–2136 (2018).
- Baldi, P., Sadowski, P. & Whiteson, D. Searching for exotic particles in high-energy physics with deep learning. *Nature Communications* **5**, 4308 (2014).
- Gebhardt, R. S., Du, P., Wodo, O. & Ganapathysubramanian, B. A data-driven identification of morphological features influencing the fill factor and efficiency of organic photovoltaic devices. *Computational Materials Science* **129**, 220–225 (2017).
- Singh, R. *et al.* Physics-aware deep generative models for creating synthetic microstructures. *arXiv preprint arXiv:1811.09669* (2018).
- Pokuri, B. S. S., Ghosal, S., Kokate, A., Sarkar, S. & Ganapathysubramanian, B. Interpretable deep learning for guided microstructure-property explorations in photovoltaics. *npj Computational Materials* **5**, 1–11 (2019).
- Esteva, A. *et al.* Dermatologist-level classification of skin cancer with deep neural networks. *Nature* **542**, 115 (2017).
- Ghosal, S. *et al.* An explainable deep machine vision framework for plant stress phenotyping. *Proceedings of the National Academy of Sciences* **115**, 4613–4618 (2018).
- Daily, M., Medasani, S., Behringer, R. & Trivedi, M. Self-driving cars. *Computer* **50**, 18–23 (2017).
- Valipour, S. *Deep Learning in Robotics*. Ph.D. thesis, University of Alberta (2017).
- Ghadai, S., Balu, A., Sarkar, S. & Krishnamurthy, A. Learning localized features in 3D CAD models for manufacturability analysis of drilled holes. *Computer Aided Geometric Design* **62**, 263–275 (2018).
- Lore, K. G., Stoecklein, D., Davies, M., Ganapathysubramanian, B. & Sarkar, S. A deep learning framework for causal shape transformation. *Neural Networks* **98**, 305–317 (2018).
- Akintayo, A., Lore, K. G., Sarkar, S. & Sarkar, S. Prognostics of combustion instabilities from hi-speed flame video using a deep convolutional selective autoencoder. *International Journal of Prognostics and Health Management* **7**, 1–14 (2016).
- Hsu, M.-C. *et al.* Dynamic and fluid–structure interaction simulations of bioprosthetic heart valves using parametric design with T-splines and Fung–type material models. *Computational Mechanics* **55**, 1211–1225 (2015).
- Capps, S. B., Elkins, R. C. & Fronk, D. M. Body surface area as a predictor of aortic and pulmonary valve diameter. *The Journal of thoracic and cardiovascular surgery* **119**, 975–982 (2000).
- Maaten, L. V. D. & Hinton, G. Visualizing data using t-SNE. *Journal of Machine Learning Research* **9**, 2579–2605 (2008).
- Kou, S. *et al.* Echocardiographic reference ranges for normal cardiac chamber size: results from the NORRE study. *European Heart Journal - Cardiovascular Imaging* **15**, 680–690, <https://doi.org/10.1093/ehjci/jet284>, <http://oup.prod.sis.lan/ehjci/article-pdf/15/6/680/7140445/jet284.pdf> (2014).
- Wang, N. & Yeung, D.-Y. Learning a deep compact image representation for visual tracking. In *Advances in neural information processing systems*, 809–817 (2013).
- Krizhevsky, A. & Hinton, G. E. Using very deep autoencoders for content-based image retrieval. In *European Symposium on Artificial Neural Networks (ESANN)* (2011).
- Pu, Y. *et al.* Variational autoencoder for deep learning of images, labels, and captions. In *Advances in Neural Information Processing Systems*, 2352–2360 (2016).
- Goodfellow, I. *et al.* Generative adversarial nets. In *Advances in Neural Information Processing Systems*, 2672–2680 (2014).
- Bronstein, M. M., Bruna, J., LeCun, Y., Szlam, A. & Vandergheynst, P. Geometric deep learning: Going beyond Euclidean data. *IEEE Signal Processing Magazine* **34**, 18–42 (2017).
- LeCun, Y., Bottou, L., Bengio, Y. & Haffner, P. Gradient-based learning applied to document recognition. *Proceedings of the IEEE* **86**, 2278–2324 (1998).
- Bhatnagar, S., Afshar, Y., Pan, S., Duraisamy, K. & Kaushik, S. Prediction of aerodynamic flow fields using convolutional neural networks. *Computational Mechanics* 1–21 (2019).
- Lee, S. & You, D. Data-driven prediction of unsteady flow fields over a circular cylinder using deep learning. *arXiv preprint arXiv:1804.06076* (2018).
- Prantl, L., Bonev, B. & Thuerey, N. Generating liquid simulations with deformation-aware neural networks. *arXiv preprint arXiv:1704.07854* (2017).
- Holland, J. R., Baeder, J. D. & Duraisamy, K. Field inversion and machine learning with embedded neural networks: Physics-consistent neural network training. In *AIAA Aviation 2019 Forum*, 3200 (2019).

45. Teichert, G. H. & Garikipati, K. Machine learning materials physics: Surrogate optimization and multi-fidelity algorithms predict precipitate morphology in an alternative to phase field dynamics. *Computer Methods in Applied Mechanics and Engineering* **344**, 666–693 (2019).
46. Shah, V. *et al.* Encoding invariances in deep generative models. *arXiv preprint arXiv:1906.01626* (2019).
47. Zhang, D., Guo, L. & Karniadakis, G. E. Learning in modal space: Solving time-dependent stochastic pdes using physics-informed neural networks. *arXiv preprint arXiv:1905.01205* (2019).
48. Lu, L., Meng, X., Mao, Z. & Karniadakis, G. E. Deepxde: A deep learning library for solving differential equations. *arXiv preprint arXiv:1907.04502* (2019).
49. Jagtap, A. D. & Karniadakis, G. E. Adaptive activation functions accelerate convergence in deep and physics-informed neural networks. *arXiv preprint arXiv:1906.01170* (2019).
50. Zhang, D., Lu, L., Guo, L. & Karniadakis, G. E. Quantifying total uncertainty in physics-informed neural networks for solving forward and inverse stochastic problems. *Journal of Computational Physics* (2019).
51. Pan, S. & Duraisamy, K. Physics-informed probabilistic learning of linear embeddings of non-linear dynamics with guaranteed stability. *arXiv preprint arXiv:1906.03663* (2019).
52. Liang, L., Liu, M. & Sun, W. A deep learning approach to estimate chemically-treated collagenous tissue nonlinear anisotropic stress-strain responses from microscopy images. *Acta biomaterialia* **63**, 227–235 (2017).
53. Liang, L., Liu, M., Martin, C. & Sun, W. A deep learning approach to estimate stress distribution: A fast and accurate surrogate of finite-element analysis. *Journal of The Royal Society Interface* **15**, 20170844 (2018).
54. Aranda, A. & Valencia, A. Study on cerebral aneurysms: Rupture risk prediction using geometrical parameters and wall shear stress with cfd and machine learning tools. *Machine Learning and Applications: An International Journal (MLAIJ) Vol 5* (2018).
55. Liu, M., Liang, L. & Sun, W. Estimation of *in vivo* constitutive parameters of the aortic wall: a machine learning approach. *bioRxiv* 366963 (2018).
56. Liu, M., Liang, L. & Sun, W. Estimation of *in vivo* constitutive parameters of the aortic wall using a machine learning approach. *Computer methods in applied mechanics and engineering* **347**, 201–217 (2019).
57. Travaglino, S. *et al.* Computational optimization study of transcatheter aortic valve leaflet design using porcine and bovine leaflets. *Journal of biomechanical engineering* **142** (2020).
58. Li, K. & Sun, W. Simulated transcatheter aortic valve deformation: A parametric study on the impact of leaflet geometry on valve peak stress. *International journal for numerical methods in biomedical engineering* **33**, e02814 (2017).
59. Liang, L. *et al.* Machine learning-based 3D geometry reconstruction and modeling of aortic valve deformation using 3D computed tomography images. *International journal for numerical methods in biomedical engineering* **33**, e2827 (2017).
60. Kissas, G. *et al.* Machine learning in cardiovascular flows modeling: Predicting pulse wave propagation from non-invasive clinical measurements using physics-informed deep learning. *arXiv preprint arXiv:1905.04817* (2019).
61. Maher, G., Wilson, N. & Marsden, A. Accelerating cardiovascular model building with convolutional neural networks. *Medical & biological engineering & computing* 1–17 (2019).
62. Maturana, D. & Scherer, S. VoxNet: A 3D convolutional neural network for real-time object recognition. In *International Conference on Intelligent Robots (IROS)* (2015).
63. Riegler, G., Ulusoy, A. O. & Geiger, A. Octnet: Learning deep 3D representations at high resolutions. In *Proceedings of the IEEE Conference on Computer Vision and Pattern Recognition*, vol. 3 (2017).
64. Ghadai, S., Lee, X., Balu, A., Sarkar, S. & Krishnamurthy, A. Multi-resolution 3D convolutional neural networks for object recognition. *arXiv preprint arXiv:1805.12254* (2018).
65. Qi, C. R., Yi, L., Su, H. & Guibas, L. J. Pointnet++: Deep hierarchical feature learning on point sets in a metric space. In *Advances in Neural Information Processing Systems*, 5105–5114 (2017).
66. Krishnamurthy, A., Khardekar, R. & McMains, S. Optimized GPU evaluation of arbitrary degree NURBS curves and surfaces. *Computer-Aided Design* **41**, 971–980 (2009).
67. Lore, K. G., Akintayo, A. & Sarkar, S. LLNet: A deep autoencoder approach to natural low-light image enhancement. *Pattern Recognition* **61**, 650–662 (2017).
68. Wong, S. C., Gatt, A., Stamatescu, V. & McDonnell, M. D. Understanding data augmentation for classification: When to warp? In *2016 International Conference on Digital Image Computing: Techniques and Applications (DICTA)*, 1–6 (2016).

Acknowledgements

This work was partly supported by the NSF under grant number CMMI:1644441 (A.K., S.S. and A.B.), and OAC:1750865 (A.K.), and NIH/NHLBI Grants R01HL129077 and R01HL142504 (S.N., F.X. and M.C.H.). The computations were performed using the Nova Cluster at Iowa State University, which is funded by NSF MRI grant 1726447.

Author contributions

A.K., M.C.H. and S.S. initiated the project; A.K. and M.C.H. planned data collection and analysis process. S.S. designed the ML framework; A.B., F.X. and S.N. performed the training, and analyzed the data; all authors contributed to writing the manuscript. The authors declare no conflict of interest.

Competing interests

The authors declare no competing interests.

Additional information

Supplementary information is available for this paper at <https://doi.org/10.1038/s41598-019-54707-9>.

Correspondence and requests for materials should be addressed to A.K.

Reprints and permissions information is available at www.nature.com/reprints.

Publisher's note Springer Nature remains neutral with regard to jurisdictional claims in published maps and institutional affiliations.



Open Access This article is licensed under a Creative Commons Attribution 4.0 International License, which permits use, sharing, adaptation, distribution and reproduction in any medium or format, as long as you give appropriate credit to the original author(s) and the source, provide a link to the Creative Commons license, and indicate if changes were made. The images or other third party material in this article are included in the article's Creative Commons license, unless indicated otherwise in a credit line to the material. If material is not included in the article's Creative Commons license and your intended use is not permitted by statutory regulation or exceeds the permitted use, you will need to obtain permission directly from the copyright holder. To view a copy of this license, visit <http://creativecommons.org/licenses/by/4.0/>.

© The Author(s) 2019

A Deep Learning Framework for Design and Analysis of Surgical Bioprosthetic Heart Valves

Supplementary Material

Aditya Balu, Sahiti Nallagonda, Fei Xu, Adarsh Krishnamurthy*, Ming-Chen Hsu, Soumik Sarkar
Iowa State University, Department of Mechanical Engineering, Ames, 50011, US

NURBS-based modeling of surfaces

Non-Uniform Rational B-spline (NURBS) surfaces are the most general parametric representation of smooth surfaces. NURBS surfaces are represented using a set of weighted control points and two knot vectors, one for each parametric direction, u and v . The knot vectors control the parametric spacing between the control points. Intuitively, the NURBS surfaces can be thought as a smooth surface approximation guided by the control points, whose continuity is controlled by the knot vectors, and the relative importance of the control points by the weights.

Mathematically, NURBS are a generalization of B-splines. The NURBS surface is defined by a $m \times n$ control points mesh, $P_{i,j}$ with corresponding weights $w_{i,j}$; two parametric directions, u and v with their associated knot vectors, degrees (p and q), and basis functions, $N_{i,p}(u)$ and $N_{j,q}(v)$. The knot vector is a set of parametric coordinates which divide the B-Spline into piecewise sections. If the knot intervals are equal, the spline is considered uniform. The basis functions are defined using the Cox-de Boor recursion formula⁹:

$$N_{i,p}(u) = \frac{u - u_i}{u_{i+p} - u_i} N_{i,p-1}(u) + \frac{u_{i+p+1} - u}{u_{i+p+1} - u_{i+1}} N_{i+1,p-1}(u) \quad (1)$$

with

$$N_{1,p}(u) = \begin{cases} 0, & \text{if } u_i \leq u \leq u_i + 1 \\ 1, & \text{otherwise} \end{cases} \quad (2)$$

NURBS surfaces are a generalization of B-spline surfaces with the addition of weights, $w_{i,j}$, assigned to each control point, $P_{i,j}$. The basis functions are modified to be

$$R_{i,j}^{p,q}(u, v) = \frac{N_{i,p}(u) N_{j,q}(v) w_{i,j}}{\sum_{k=0}^n \sum_{l=0}^m N_{k,p}(u) N_{l,q}(v) w_{k,l}}. \quad (3)$$

The NURBS surface is defined as:

$$S(u, v) = \sum_{i=0}^n \sum_{j=0}^m R_{i,j}^{p,q}(u, v) P_{i,j}. \quad (4)$$

Learning from NURBS representation

Any machine learning framework requires careful selection of three main components: (i) data representation, (ii) model architecture, and (iii) training algorithm. For effective learning, the domain knowledge needs to be embedded in each component. In convolutional neural networks for image recognition, one embeds the spatial localization using the convolution filters (model architecture) and the pixels of the image are represented using multiple red-green-blue-alpha channels (data representation)^{6,7}. For design for manufacturing application, embedding the CAD models in a voxel-based representation was required to learn the volumetric features using 3D convolution filters (model architecture)³. Note that sophisticated model architectures are not essential to train the machine learning network in these problems; these could be trained by using basic dense neural networks. However, the data and time requirements for learning such dense network increases combinatorially. Therefore, the chosen approach of NURBS-aware Convolution is necessary for effectively learning from the NURBS CAD representation. A simple demonstration of

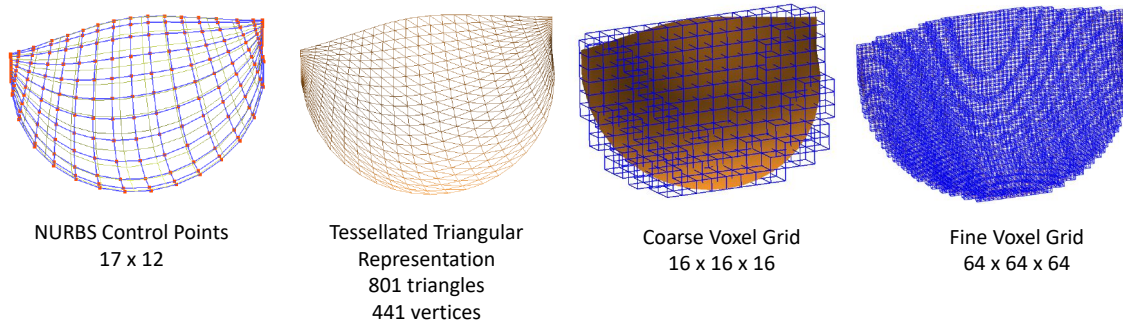


Figure A1: The different representations of a leaflet of the heart valve and their dimensionality. The representation using the control points is the most succinct and sound representation among all.

the effectiveness is shown in [Figure A1](#). It can be easily understood that the dimensionality of the NURBS-aware convolution operation is lower than other representations and hence the data requirements are also lower. At the same time, any representation other than the direct usage of control points also involves some loss of information. For example, a coarse level voxel grid may not be able to capture all the features of the leaflet. However, a lossless representation of the geometry is necessary for understanding several key notions of biomechanics, such as contact. A fine level voxel grid might be a possible candidate; however, the dimensionality increases by a factor of ≈ 500 .

In addition, data augmentation is necessary¹⁰ for successfully learning the network weights. There are other approaches where the phenomena can be embedded in the algorithm to enable faster learning. In this study, we exploit these approaches of embedding the physical valve characteristics in the machine learning model to learn the deformation mechanics of heart valves.

Parametric design of heart valve

The aorta is the largest blood vessel that carries blood from the heart to the rest of the body. The aortic valve—one of the four heart valves—is located between the left ventricle and the left aorta. The aortic root represents the connection between the aorta and myocardium: it consists of the sinuses, the aortic valve leaflets, the commissures, and the interleaflet triangles. The three leaflets (left coronary leaflet, right coronary leaflet and non-coronary leaflet) form the aortic valve and provide its main sealing mechanism. The anatomy of the BHV leaflet can be divided into three parts, first, the free edge which provides sealing by forming contact with the neighboring leaflets to form a seal (the area of contact is called the coaptation area). Second, The “belly” of the leaflet and third, the bottom parts of leaflet or leaflet attachments. The aortic valve leaflets form the junction and physical boundary between the left ventricle and aorta.

Surgical BHVs considered in this work are fabricated from bovine and porcine pericardium sheets that are chemically fixed *after* being die-cut and mounted onto a metal frame to form the leaflets. As a result, the geometry shown in [Figure A2](#) is without internal stresses and can be used directly as the stress-free configuration. The leaflet is initially flat in 2D before being mounted onto the metal frame. However, the non-flat leaflet in 3D represents the working condition of the BHVs and the analysis is performed using this configuration. In order to find the flat leaflet that can deform and then perfectly match the designed 3D shape, one can perform an inverse design simulation to reverse the process and iteratively find the 2D flat shape from the 3D shape.

The parametric design of a heart valve is divided into two steps; step (i) we define the size of the valve for a given aortic root, and step (ii) we define the shape parameters of the heart valve that define the geometry without any dependency on the size of the aortic root. The valve leaflets are parametrized using the aortic root as basis, First, 9 key registration points located on the ends of commissure lines at the bottom of the sinuses are identified. These define the attachment points of the leaflets to the sinuses, indicated by blue spheres in [Figure A2](#). These key points are derived from the patient specific aortic root and will not change for different valve designs. The univariate B-splines are parametrized to define the free edges and belly

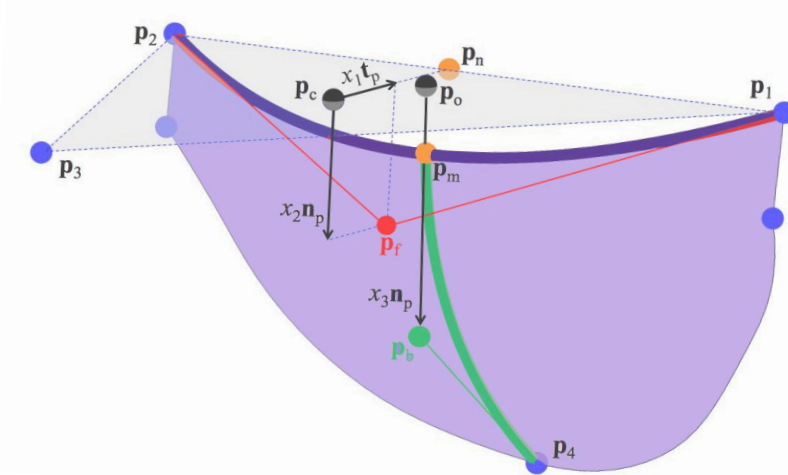


Figure A2: Parametric design of bioprosthetic heart valves.

curves of the leaflet, shown in red and green respectively in the figure. A smooth B-Spline representation of the leaflet is obtained by interpolation of the attachment edges, free edges, and belly curves. In Figure A2, p_1, p_2, p_3 are the key points on the top of commissure line and p_4 is the key point on the bottom of the sinus. P_1 to p_3 define a triangle with p_c being its geometric center. t_p is the unit vector pointing from p_c to p_n (geometric center of p_1 and p_2), and the unit normal vector of the triangle p_{1-3} pointing downwards in n_p . The free edge is constructed as a univariate quadratic B-spline curve determined by 3 control points, p_1, p_f and p_2 . p_f is defined as $p_c + x_1 t_p + x_2 n_p$. By changing x_1 and x_2 to control the location of p_f , the curvature (length) and the height of the free edge can be parametrically modified. We then take p_m as the midpoint of the free edge, the point p_b , and the key point p_4 to construct a univariate quadratic B-spline curve (green). In this model, x_1, x_2 , and x_3 can be chosen as design variables to parametrically change the free edge and belly curve and therefore, parametrically control the valve design. This procedure is implemented in Rhino/Grasshopper refer to Xu et. al.¹² for more details of parametric model.

Isogeometric analysis

The generation of data for training the DLFEA is performed using isogeometric shell analysis. Isogeometric analysis (IGA)⁴ is an extremely useful tool in analyzing NURBS-based geometry by extending the finite element formulation to use the same NURBS basis functions for the analysis. The major advantage of IGA over traditional finite element method is that it does not require the geometry to be meshed, which is both tedious and causes loss of information due to mesh approximation. IGA has been proven to be useful for valvular analysis by several researchers^{5,8}.

Formulation

We perform dynamic simulations of pericardial BHV function at its closure with a prescribed transvalvular pressure load. The dynamic simulations are performed using Kirchoff-Love shell theory and Lee-Sacks material constitutive model (isotropic) (explained below). With the prescribed material properties and transvalvular pressure, we perform dynamic simulations while modeling the viscous and inertial resistance of the surrounding fluid using damping⁵. We perform the valve closure simulations by slowly ramping up the pressure to the prescribed transvalvular pressure in 100 time steps with a time step size of 0.0001 s. Then, with constant pressure, we run more steps till a steady-state valve closure is achieved. The damping coefficient is kept very high in order to quickly stabilize the ramp up of pressure. In the context of this paper, we perform valve closure simulations using structural simulations. Since the valve is closed, the structural analysis of heart valves will model the behavior very well (i.e. a hydrostatic state of stress exists and there is no flow). More advanced study of the behavior of heart valve may require fluid-structure interaction (FSI) simulations which involves temporal dynamics of blood flow for the complete cycle of the heart.

Material parameters

Kiendl et al.⁵ built a generic Kirchoff-love shell theory for materials of this type and also provide a case study with an exponential-type isotropic model for strain energy function, ψ_{el} .

$$\psi_{el} = \frac{c_0}{2}(I_1 - 3) + \frac{c_1}{2}(e^{c_2(I_1-3)^2} - 1) \quad (5)$$

Here, I_1 is the first invariant of the right Cauchy–Green deformation tensor, \mathbf{C} . The magnitude of the parameters c_0 , c_1 , c_2 depends on the chemical treatment for the BHVs. The material is assumed to be incompressible, which is done by augmenting the elastic strain-energy function, ψ_{el} with a constraint term to enforce $J = \sqrt{\det(\mathbf{C})} = 1$, via a Lagrange multiplier p : $\psi = \psi_{el} - p(J - 1)$. In addition, the thickness of the leaflets is another key material property that changes the deformation behavior.

Dynamic simulations and convergence

While the default parameters for damping, time steps, and time step size, are as mentioned above, insufficient damping can lead to a large residual while ramping up to a particular prescribed material properties or transvalvular pressure from the reference configuration of the geometry. In addition, insufficient damping can also cause oscillations in the deformed geometry, leading to oscillations in the coaptation area and contact. Therefore, successful convergence of a particular simulation depends on carefully adjusting the parameters such as damping coefficient, time steps, time step size, etc. While generating the samples for training, since these parameters are dependent on each simulation, a generic set of parameters that would work for most of the simulations is used as default; specific cases of non-convergence are manually addressed by changing these parameters.

Mesh convergence

While the convergence of the individual simulations is important, the mesh resolution used for generating the simulation results is also important. In order to have an accurate solution for the valve deformation and to compute the coaptation area accurately, we performed a study on the convergence of the coaptation area with mesh resolution. We performed this study by choosing a representative bioprosthetic aortic valve with known geometry parameters and obtained different mesh representations of the NURBS surface to be used for isogeometric analysis. [Figure A3](#) shows the computed coaptation area for different number of cubic elements corresponding to the mesh used for analysis. Based on this, we chose to create a representative NURBS patch using 17×12 control points for each leaflet. We observe that the coaptation area for this representative geometry in the chosen mesh resolution is 1.0116 cm^2 , while the value for a finer resolution is 1.0541 cm^2 . There is a 4% deviation in the coaptation area computed using our chosen resolution with respect to the finer resolution. This deviation in the coaptation area is acceptable, which balances the computational time with simulation accuracy. While increasing the resolution might improve the accuracy in the biomechanics simulations, it also increases the time taken for generating the data and simulations. Therefore, we use the chosen resolution for generating the data.

Data generation

The inputs to the DLFEA are (1) reference geometry, (2) the transvalvular aortic pressure and (3) material properties (c_0 , c_1 , c_2 , thickness). Varying them to cover all kinds of material variations and all kinds of physiological conditions of different patients is necessary. Therefore, we use the list of thicknesses in the physiological region by choosing thicknesses provided in Section 3.1 of Caballero et al.². Similarly, we vary other material properties by choosing the physiologically prescribed value given in Wu et. al.¹¹ and then varying them from 80% to 120% of that value. The geometries are obtained by changing the parameters provided in [Table A1](#). Several simulations were run with different values for the valve thickness, material properties, aortic pressure, and geometric parameters such as belly curve parameter, height of the free edge, etc.

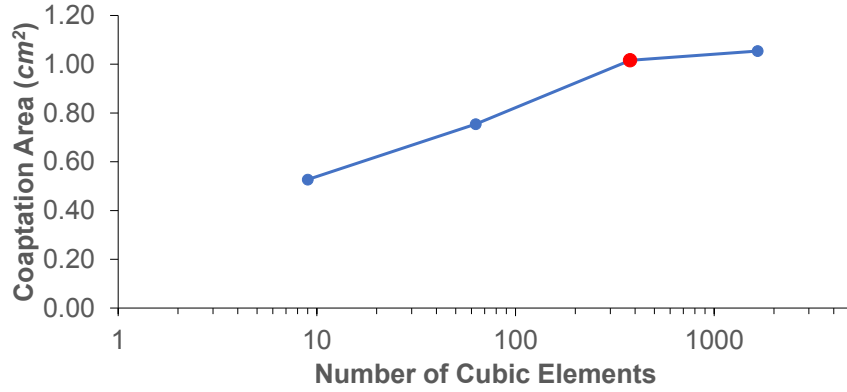


Figure A3: Study of the convergence of the coaptation area with mesh resolution for a representative bioprosthetic aortic valve. The mesh resolution chosen for DLFEA data generation is marked in red.

Parameter	Min. Value	Max. Value	Number of Values
Free Edge Curve Parameter (cm)	0.05	0.45	3
Belly Curve Parameter (cm)	0.2	1.4	7
Height of the Free Edge (cm)	-0.1	0.5	4
thickness (mm)	0.186	0.427	5
c_0 (kPa)	54.084	81.130	3
c_1 (kPa)	10.628	15.942	3
c_2	30.554	45.826	3

Table A1: Parameters used for generating the reference geometries and material parameters required for training.

Training

A total of 90,941 simulations converged with the default simulation parameters and were used for the training of the network. From the total data samples generated, a part of data is reserved for validation and for testing of the model for its generalization capability. The validation data is used to tune the hyperparameters of the network, where we optimize the number of convolution layers, number of fully-connected layers, number of channels in each of the convolution layers, number of neurons in each fully connected layer, etc. Using the validation data, we could ensure that we choose the best hyperparameters that produce the least

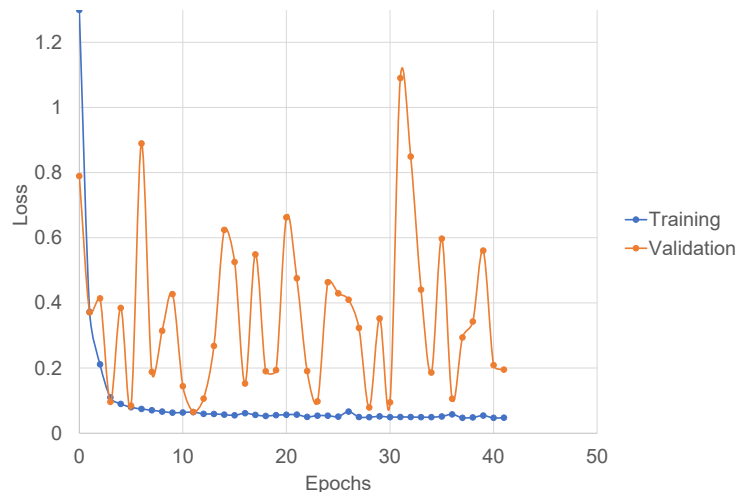


Figure A4: Training and validation loss characteristics with respect to epochs. The weights with minimum validation loss are stored for performing inference and other tests and visualizations.

Common Training Parameters	DLFEA Architecture Block	Hyperparameters
Batch Size: 512 Optimizer: Adam	Encoder	Convolutional layer 1 (3 filters with size 5×5)
		Convolutional layer 2 (8 filters with size 3×3)
	Repetitions of scalars	Convolutional layer 3 (16 filters with size 3×3)
		Convolutional layer 3 (32 filters with size 3×3)
	Code layer	Pressure: 20
Decoder	Code layer	Thickness: 20
		Fully connected layer 1(64 neurons)
	Decoder	Fully connected layer 2(48 neurons)
		Deconvolution start size ($8 \times 9 \times 4$)
		Deconvolution layer 1 (8 filters with size 5×5)
Decoder	Deconvolution layer 2 (6 filters with size 3×3)	
	Deconvolution layer 3 (6 filters with size 3×3)	
Decoder	Deconvolution layer 4 (4 filters with size 3×3)	
Decoder	Deconvolution layer 5 (3 filters with size 1×1)	

Table A2: Optimized hyperparameters with the least validation loss.

loss with not just the training data, but also with the validation data. However, to be fair in evaluating the performance of the model, it is a good practice to have a test of the performance on data that is not used for training and hyperparameter optimization. This proves the generalization of the data over the complete range of the input cases.

The training and validation loss variation with epochs for training is shown in [Figure A4](#). In general, we save the weights of the model with least validation loss. We run for 30 additional epochs to check if the loss reduces further. In the [Figure A4](#), we see that at the 11th epoch the training and validation loss are very close to each other and validation loss is minimum. Yet, we still run for 30 more epochs to ensure that the

Algorithm 1: Training Algorithm

Input : Network Architecture

Initialize: Weights for all layers, $W_l, (l = 1, 2, \dots, m)$; patience = 0

Load Data: Load training data \mathcal{D} and validation data \mathcal{D}_V

```

for ( $i = 0; i \leq num\_epochs; i++$ ) do
  Randomly shuffle the data
  Split  $\mathcal{D}$  to  $\mathcal{D}_j, (j = 1, 2, \dots, n)$  mini-batches
  for  $j = 1 : n$  do
    Predict outputs  $\mathcal{O}_j$  for mini-batch  $\mathcal{D}_j$ 
    Compute loss  $\mathcal{L}(\mathcal{D}_j, \mathcal{O}_j, \{W\})$ 
    Update weights,  $\{W\}$  using Adam optimizer
  end
  Predict validation outputs  $\mathcal{O}_V$  for  $\mathcal{D}_V$ 
  Compute Validation Loss  $\mathcal{L}(\mathcal{D}_V, \mathcal{O}_V, \{W\})$ 
  if Avg. Validation Loss not improving then
    | increment patience
  end
  else
    | patience = 0
  end
  if  $patience \geq 30$  then
    | Exit
  end
end

```

weights obtained are truly minimal and has good generalization capability. Finally, we stop at the end of 42 epoch because we do not find any better weights with a lower validation loss. The sum training loss for all the predicted outputs is 0.0594 and the validation loss is 0.0495 for the plot shown. The corresponding test loss is also of the same order due to the model having a good generalization capability. The final hyperparameters of the network (i.e. the number of convolution layers, number of convolution filters, the filter size, the code layer size, etc.) are shown in [Table A2](#). The overall training procedure for a given set of hyperparameters is shown in [Algorithm 1](#).

Statistical analysis

Error measurements

Two major metrics were used while comparing the results: (i) the root mean-squared error, and (ii) the correlation coefficient. The root mean-squared error is computed by:

$$RMSE = \sqrt{\frac{\sum_i^k (p_1 - p_2)^2}{N}}$$

The correlation coefficient (more popularly known as Pearson Correlation Coefficient, R), which was used for the comparison of the results is given by:

$$R = \frac{cov(x, y)}{\sigma_x \sigma_y},$$

where $cov(x, y)$ is the covariance between x and y and σ is the standard deviation.

A simpler formula used for computing is as follows:

$$R = \frac{\sum (x - m_x)(y - m_y)}{\sqrt{\sum (x - m_x)^2 \sum (y - m_y)^2}}.$$

Here m_x and m_y represent the mean of vectors x and y .

Distance measures between two 3D objects

Euclidean distance between two points p, q in N-Dimensional space is given by

$$d(\mathbf{p}, \mathbf{q}) = \sqrt{(p_1 - q_1)^2 + (p_2 - q_2)^2 + \dots + (p_N - q_N)^2}$$

By distance between two CAD representations, we refer to the mean of the euclidean distances of samples points in the surface of the representation. i.e. For a NURBS representation, we sample the points (say, M) for by varying the parameters u, v and evaluate the surface representation to obtain a set $\mathcal{P} = \{P^1, P^2, P^3, \dots, P^M\}$. Similarly, we could obtain another set $\mathcal{Q} = \{Q^1, Q^2, Q^3, \dots, Q^M\}$ for the other object. Distance Measures are made using the sets \mathcal{P} and \mathcal{Q} . Note that, $|\mathcal{P}| = |\mathcal{Q}| = M$.

Euclidean distance

We define the Euclidean Distance to be the mean of the euclidean distances of each point in set \mathcal{P} and set \mathcal{Q} . Mathematically, we can represent it as follows:

$$\mathcal{D}_{euclidean}(\mathcal{P}, \mathcal{Q}) = \frac{1}{M} \sum_{i=1}^M d(P^i, Q^i)$$

Hausdorff distance

Directed Hausdorff distance is the maximum of all the minimum distances from the set of points \mathcal{P} to \mathcal{Q} . Symmetric Hausdorff distance is the maximum of the two directed Hausdorff distances. It represents the maximum possible deviation between two sets. Mathematically, symmetric Hausdorff distance is represented as follows:

$$\mathcal{D}_{hausdorff}(\mathcal{P}, \mathcal{Q}) = \max\left\{\sup_{P \in \mathcal{P}} \inf_{Q \in \mathcal{Q}} d(P, Q), \sup_{Q \in \mathcal{Q}} \inf_{P \in \mathcal{P}} d(P, Q)\right\}$$

Procrustes matching

Procrustes matching is a statistical tool particularly established to compare two geometric shapes while accounting for translation, rotation, and scale between them. Procrustes matching provides a metric of dissimilarity between two 3D geometries. Mathematically, the dissimilarity measure is:

$$\mathcal{D}_{procrustes}(\mathcal{P}, \mathcal{Q}) = \frac{1}{M} \sum_{i=1}^M \sqrt{P^i - \beta Q^i \tau - \mathbf{1}\gamma},$$

where β , τ , γ are the similarity parameters representing the scale factor, rotation matrix and translation shift between the two shapes. These parameters are computed using the soft-assign Procrustes algorithm, which computes the rotation angle by taking the estimates of the first and second order moments of the data. \mathcal{D} is known as the Procrustes dissimilarity measure¹ and it has the same units as the geometry. It is the residual obtained after modifying the data using the soft-assign Procrustes algorithm. The goodness of the fit is evaluated using the sum of squared errors criterion.

Additional results

The main paper shows the results for the variation of the coaptation area with material properties, pressure, and geometry. On careful examination of the variation of the coaptation area with respect to the material properties, we notice that there is not much variation of the coaptation Area with the material coefficients c_0 , c_1 , and c_2 , in the physiological range of these parameter values (see [Figure A5](#)). Therefore, we come up with another refined network with just pressure, thickness, and reference configuration as the input to DLFEA as shown in [Figure A6](#).

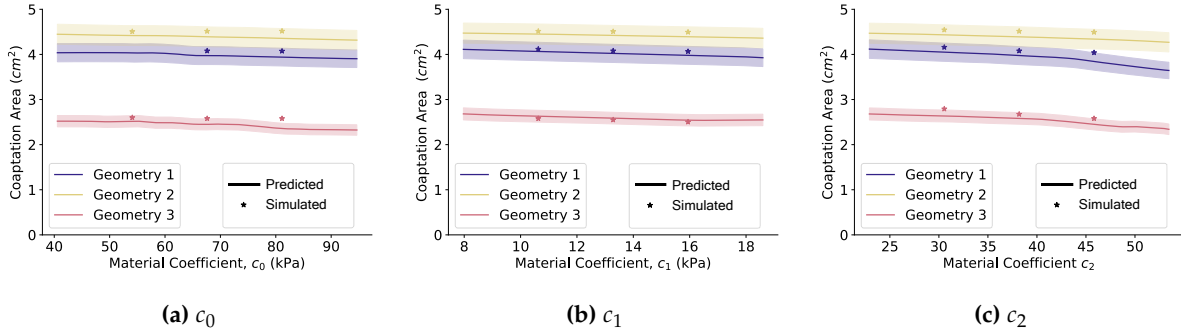


Figure A5: DLFEA-predicted coaptation area variation with the variation of different Material Coefficients. The highlighted region show 10% variation in the predicted coaptation area values.

Alternate model with fixed material parameters

As explained in the previous section, there is not much variation in the coaptation area with the material properties. Due to this observation, we explored another model with fixed material properties. However, note that, material properties does play a crucial role in the several other quantities of interest, therefore, the original model proposed is more generic and can be used to generalize for other quantities of interest. The architecture of the modified network is shown in [Figure A6](#). The training was performed with a subset

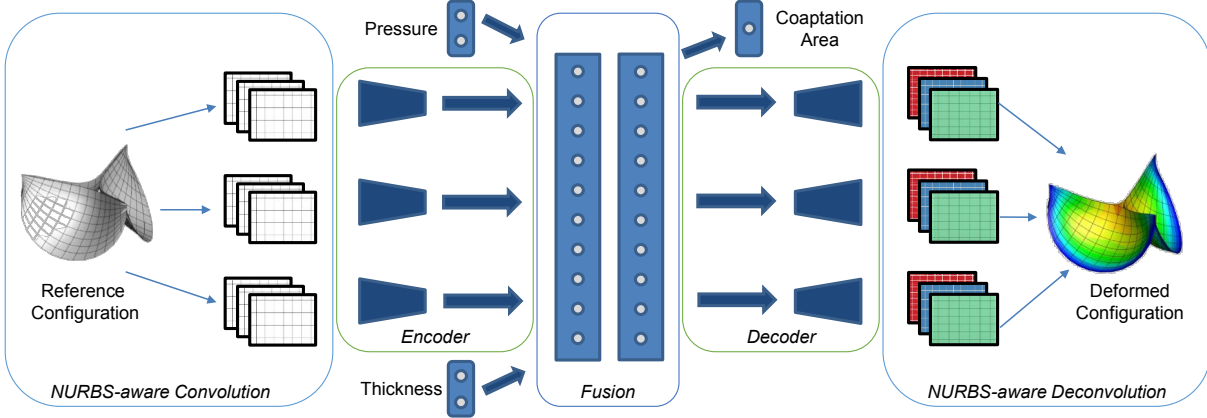


Figure A6: Alternate model of deep-learning-based convolutional autoencoder for predicting the output deformations and the coaptation area of the heart valve in the closed state, with the BHV leaflet reference geometry, thickness, and the aortic pressure as input.

Stats	Euclidean			Hausdorff			Procrustes		
	Max.	Mean	Median	Max.	Mean	Median	Max.	Mean	Median
Training	0.1509	0.0157	0.0115	0.2700	0.0652	0.0574	0.0060	0.0004	0.0003
Validation	0.1346	0.0155	0.0115	0.2568	0.0654	0.0575	0.0056	0.0004	0.0003
Test	0.1477	0.0157	0.0115	0.2689	0.0655	0.0578	0.0059	0.0004	0.0003

Table A3: Statistics on the metrics describing the prediction of deformations by the modified DLFEA. All units in cm.

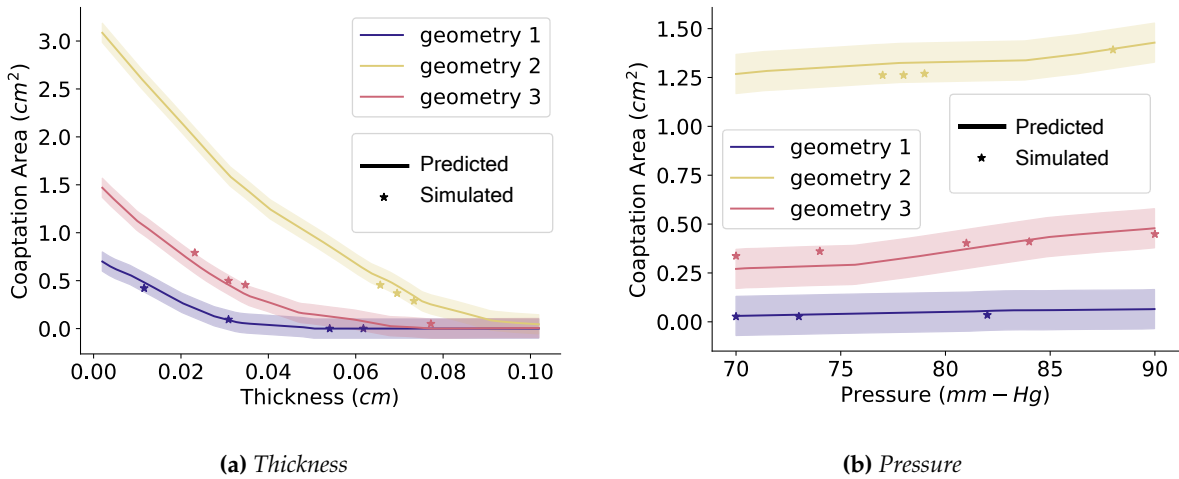


Figure A7: Figure A7b shows the DLFEA-predicted coaptation area variation with pressure for three specific sets of reference configuration geometries. Figure A7a shows a similar plot with variation in thickness for three specific reference configurations, pressure and other material properties. These plots are generated with 1000 intermediate values of the parameter of interest to get a smooth curve.

of the training set, with material coefficients fixed at the physiological meaningful values¹¹. The corresponding variation of coaptation area with thickness and pressure is shown in Figure A7. Also, we perform similar tests for statistics as the original model and obtain results shown in Figure A8. It can be seen that the trends in the result is similar to the original model with an improvement in correlation for predictions of coaptation area.

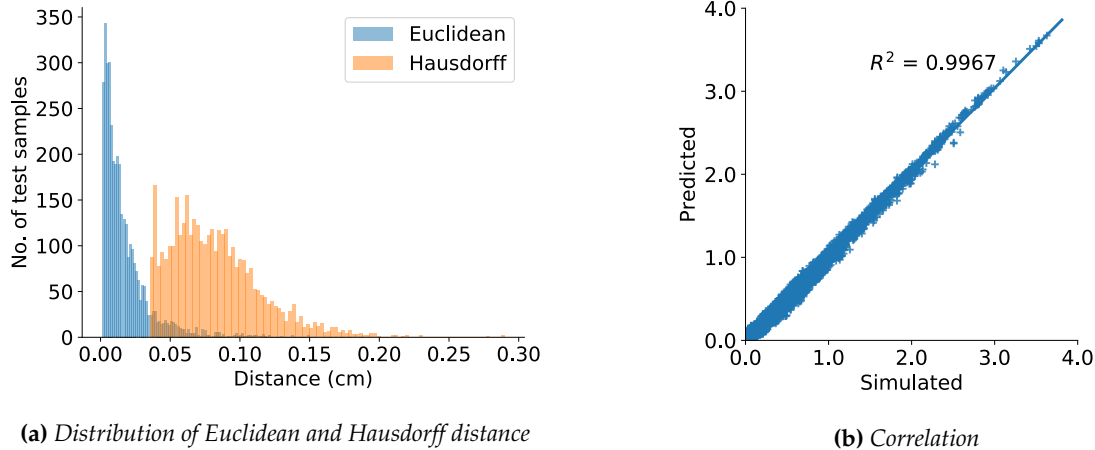


Figure A8: The histograms (Figure A8a) show the Euclidean distance and Hausdorff distance between predicted deformations from DLFEA and the simulated deformations for the test data. Figure A8b shows the DLFEA-predicted coaptation area compared with the coaptation area obtained from simulations. The predicted coaptation area is highly correlated ($R = 0.9967$) with the simulated values.

Anecdotal examples

Here, we present another set of anecdotal examples with different configurations (see Figure A9). They represent a more diverse set of examples including large and small deformations. The major deviation between the simulated and the DLFEA predicted deformations occur near the contact region, and particularly, for the cases where the deformations are low (see case 1 and 4 in Figure A9). It can be seen that the DLFEA output is more conservative than the actual simulations.

Extrapolation and interpolation capability of DLFEA

For use in design and diagnostic applications, the DLFEA must be able to accurately predict the deformation for any valve configuration that is obtained by interpolation or extrapolation of the design parameters (up to a reasonable extent). We show some additional results to highlight the extrapolation and interpolation capability of the DLFEA framework in predicting valve deformations. Since, the input geometry to DLFEA is not based on the parametric design variables but the NURBS control points, the DLFEA should be able to predict the deformations for a wide range of valve designs. For this, we perform extrapolation experiments by generating samples with different aortic root diameter, which is beyond the sizes of the Aortic root diameter used in training. Also, we change the curvature of the leaflets to the value beyond the range for the training samples. These results correspond to case a and b shown in Figure A10, where the deviation between the simulated and predicted deformations are less than 10%. In case b, the coaptation area is conservatively predicted to be 0.0 cm^2 by the DLFEA, much lower than the simulated coaptation area value of 0.0281 cm^2 . Conservative estimation of the coaptation area can be desirable in valve design applications to cull potential design parameters that might not provide the best performance. In addition to the valve geometry, the thickness and pressure values are also interpolated in case 3, showing that the predicted deformations are still within acceptable error bounds of 10%.

t-SNE analysis

We present some additional t-SNE visualizations that can help us understand how the learnt model can differentiate between the effects of different input parameters on the deformation. In the main text, we presented the t-SNE visualization colored based on the original DLFEA model. Figure A11a shows the data manifold for the modified DLFEA model with particular emphasis on the combination of parameters affecting the data manifold. These inferences are drawn by comparing and analyzing the effect of all variables by labeling each point in the data manifold based on the respective parameter value (see Figure A11b, Figure A11c, Figure A11d, Figure A11e, Figure A11f). The figure shows that certain clusters in the manifold have similar parameter value, while some clusters have a gradual variation of that parameter value. In addition, there are also interaction between the different parameters. For example, the valve thickness

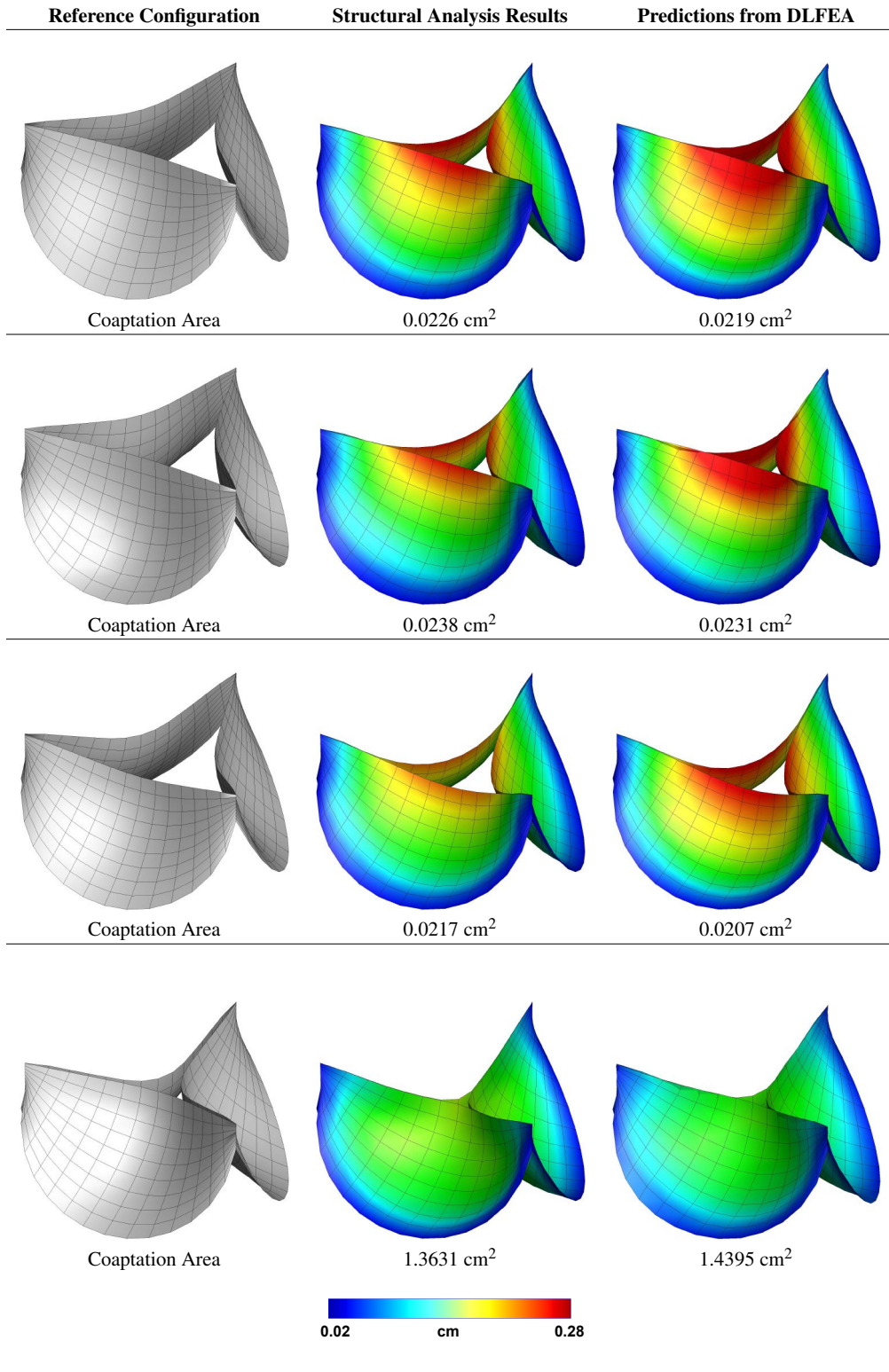


Figure A9: Illustrative examples of the valve deformations obtained from isogeometric analysis and predicted by the DLFEA framework. The simulated and predicted coaptation area is also shown below the deformations. The color in the image depicts the absolute value of the displacement in the deformed configuration of the bioprosthesis heart valve.

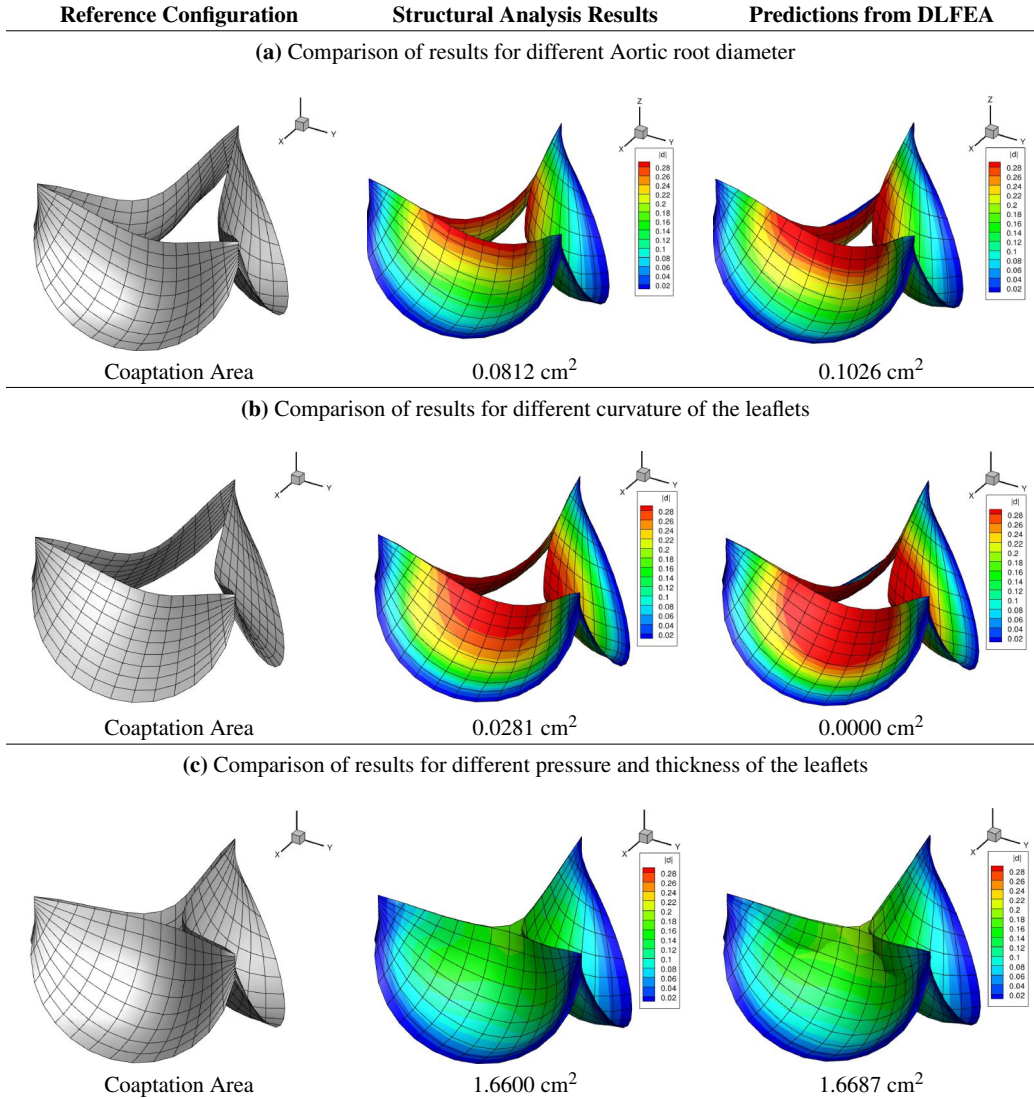
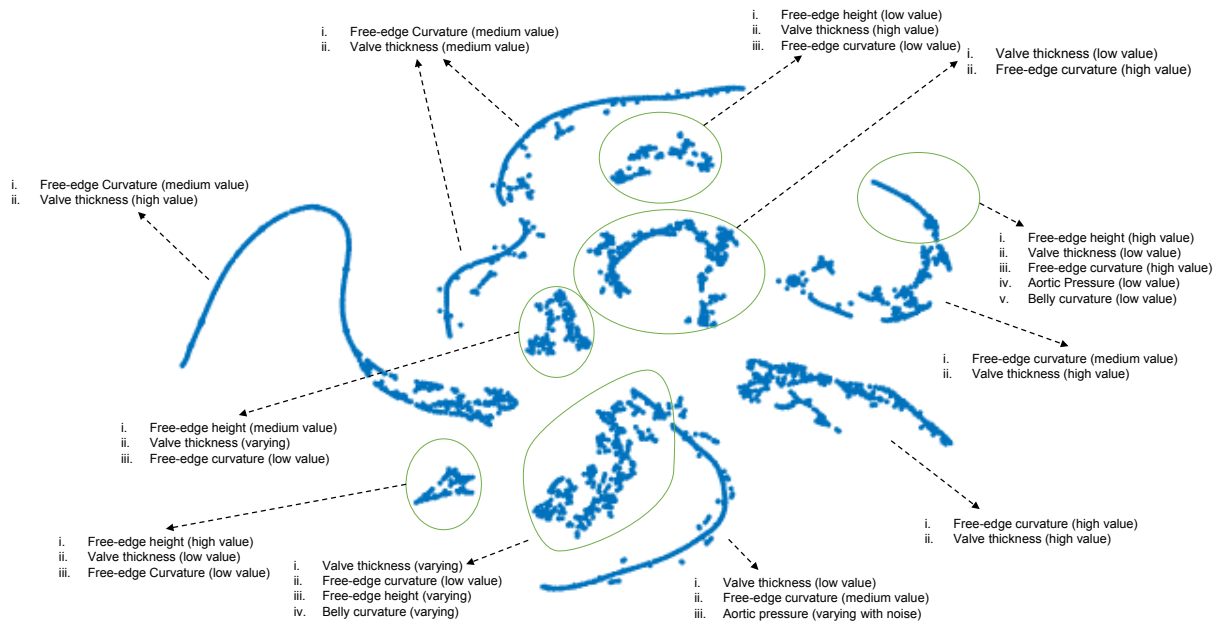


Figure A10: Generalization capability of DLFEA to predict deformations with different input parameters. The color in the image depicts the absolute value of the displacement in the deformed configuration of the bioprosthetic heart valve.

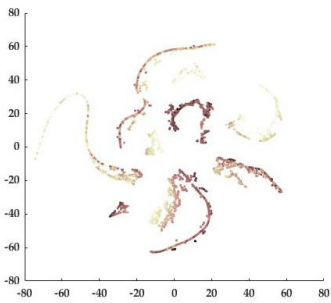
and free-edge curvature values interact; high free-edge curvature and high thickness values correlate and form a single cluster while this interaction is not significant when the free-edge curvature value is very low. Similarly, the Aortic pressure also interacts with other parameter values with low aortic pressure, low valve thickness, and high free-edge height forming a cluster. On further examination, we observe that this cluster belongs to very low or zero coaptation area. These correlation between the variables and the formation of clusters in t-SNE visualizations show that DLFEA captures the effect of each parameter on the deformations and coaptation area.

Results video

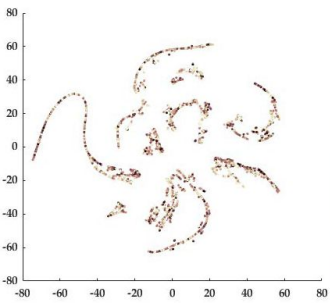
We have attached a video demonstrating the key aspects of this work. Specifically, it contains a demo of parametric design of bioprosthetic heart valves, which is discussed in detail in the first section of the Supplement. Further, we show a demonstration of a valve deformation simulation using traditional IGA and using our DLFEA framework. Finally, we visually compare the results obtained from both IGA and DLFEA.



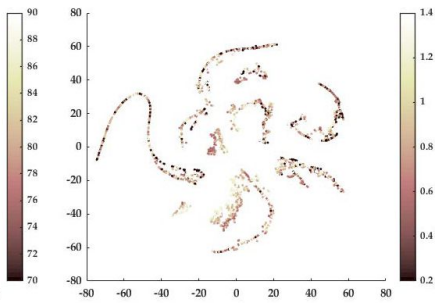
(a) *t-SNE*



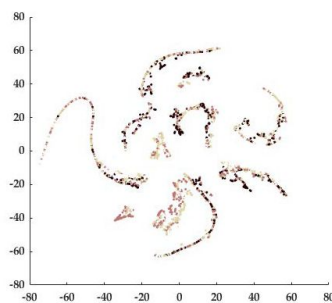
(b) *Valve thickness*



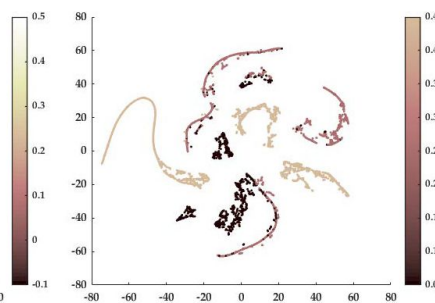
(c) *Aortic pressure*



(d) *Belly curve parameter*



(e) *Free-edge height*



(f) *Free-edge curve parameter*

Figure A11: *t*-distributed stochastic neighborhood embedding (*t*-SNE) of the higher dimensional manifold colored by the different parameters learnt by DLFEA. *t*-SNE generates a lower dimensional embedding of the data using the learnt model, which can provide insights into the distribution of the data.

References

- [1] Fred L Bookstein. *Morphometric tools for landmark data: Geometry and Biology*. Cambridge University Press, 1997.
- [2] Andrés Caballero, Fatiha Sulejmani, Caitlin Martin, Thuy Pham, and Wei Sun. Evaluation of transcatheter heart valve biomaterials: biomechanical characterization of bovine and porcine pericardium. *Journal of the mechanical behavior of biomedical materials*, 75:486–494, 2017.
- [3] Sambit Ghadai, Aditya Balu, Soumik Sarkar, and Adarsh Krishnamurthy. Learning localized features in 3D CAD models for manufacturability analysis of drilled holes. *Computer Aided Geometric Design*, 62:263–275, 2018.
- [4] T. J. R. Hughes, John A Cottrell, and Yuri Bazilevs. Isogeometric analysis: CAD, finite elements, NURBS, exact geometry and mesh refinement. *Computer Methods in Applied Mechanics and Engineering*, 194(39-41):4135–4195, 2005.
- [5] Josef Kiendl, Ming-Chen Hsu, Michael CH Wu, and Alessandro Reali. Isogeometric kirchhoff–love shell formulations for general hyperelastic materials. *Computer Methods in Applied Mechanics and Engineering*, 291:280–303, 2015.
- [6] Alex Krizhevsky, Ilya Sutskever, and Geoffrey E Hinton. Imagenet classification with deep convolutional neural networks. In F. Pereira, C. J. C. Burges, L. Bottou, and K. Q. Weinberger, editors, *Advances in Neural Information Processing Systems 25*, pages 1097–1105. Curran Associates, Inc., 2012.
- [7] Yann LeCun, Léon Bottou, Yoshua Bengio, and Patrick Haffner. Gradient-based learning applied to document recognition. *Proceedings of the IEEE*, 86(11):2278–2324, 1998.
- [8] S Morganti, F Auricchio, DJ Benson, FI Gambarin, S Hartmann, T. J. R. Hughes, and A Reali. Patient-specific isogeometric structural analysis of aortic valve closure. *Computer Methods in Applied Mechanics and Engineering*, 284:508–520, 2015.
- [9] LA Piegl and Wayne Tiller. *The NURBS book*, 1997.
- [10] S. C. Wong, A. Gatt, V. Stamatescu, and M. D. McDonnell. Understanding data augmentation for classification: When to warp? In *2016 International Conference on Digital Image Computing: Techniques and Applications (DICTA)*, pages 1–6, Nov 2016.
- [11] Michael CH Wu, Rana Zakerzadeh, David Kamensky, Josef Kiendl, Michael S Sacks, and Ming-Chen Hsu. An anisotropic constitutive model for immersogeometric fluid–structure interaction analysis of bioprosthetic heart valves. *Journal of biomechanics*, 74:23–31, 2018.
- [12] Fei Xu, Simone Morganti, Rana Zakerzadeh, David Kamensky, Ferdinando Auricchio, Alessandro Reali, T. J. R. Hughes, Michael S Sacks, and Ming-Chen Hsu. A framework for designing patient-specific bioprosthetic heart valves using immersogeometric fluid–structure interaction analysis. *International Journal for Numerical Methods in Biomedical Engineering*, 34(4):e2938, 2018.